Synthetic *In Vitro* Transcriptional Oscillators Supplementary Information

Jongmin Kim[1,4], **Erik Winfree**[2,3,4*]

1 Biology, **2** Computer Science, **3** Computation & Neural Systems, and **4** Bioengineering, California Institute of Technology, Pasadena, California, United States of America

* To whom correspondence should be addressed. E-mail: winfree@caltech.edu

Contents

1 Model equations

In this section, we first present a simple model of each transcriptional oscillator design that captures the range of dynamic behaviors each oscillator design exhibits (sections 1.1 through 1.3). For DNA and RNA hybridization and branch migration reactions, symmetry in kinetic rates were assumed for certain nucleic acids components and Hill functions were used to approximate the activation and inhibition thresholds that result from DNA and RNA hybridization and branch migration. For enzyme reactions, first-order approximations were mostly employed. We then construct a detailed model for DNA and RNA hybridization reactions and branch migration reactions, and Michaelis–Menten enzyme reactions. These mass action kinetics models (sections 1.4 through 1.6) were used to guide experimental parameter choices through optimization by random-sampling methods (1). However, for the simulation results shown in the figures of the main text and the supplementary information, we used an extended model (section 1.7) which included interference from a potential waste product in the reaction mixture.

1.1 A simple model of the two-switch negative feedback oscillator (Design I)

We introduce a 4-dimensional model, termed the 'simple model', to illustrate dynamics of a two-switch negative feedback oscillator (Design I). We take the two RNA species as dynamic signals and assume that their production rates are solely determined by the ON-state switch concentrations and their degradation rates depend only on their own concentrations. Their dynamics are given by

$$\begin{aligned} \frac{d[\mathrm{rA1}]}{dt} &= k_p \cdot [\mathrm{T12A2}] - k_d \cdot [\mathrm{rA1}], \\ \frac{d[\mathrm{rI2}]}{dt} &= k_p \cdot [\mathrm{T21A1}] - k_d \cdot [\mathrm{rI2}], \end{aligned}$$

where k_p is the production rate from an ON-state switch and k_d is the degradation rate for RNA species. The steady-state switch response to RNA inputs can be reasonably approximated by Hill functions with Hill exponents $n \approx m \approx 5$ and with thresholds set by the concentration of the strands competing for the activator (2). We observed that the half-lives of hybridization reactions are typically on the order of a few minutes in the experiments. These half-lives are consistent with two nucleic acid species, say T12A2 and rI2, at tens of nM going through a displacement reaction at about 10^5/M/s. Thus, the switch states can be modeled to follow RNA input changes with relaxation time τ as follows:

$$\begin{aligned} \frac{d[\mathrm{T12A2}]}{dt} &= \frac{1}{\tau}\left([\mathrm{T12}^{\mathrm{tot}}] \frac{1}{1+\left(\frac{[\mathrm{rI2}]}{K_I}\right)^n} - [\mathrm{T12A2}] \right), \\ \frac{d[\mathrm{T21A1}]}{dt} &= \frac{1}{\tau}\left([\mathrm{T21}^{\mathrm{tot}}] \left(1 - \frac{1}{1+\left(\frac{[\mathrm{rA1}]}{K_A}\right)^m} \right) - [\mathrm{T21A1}] \right), \end{aligned}$$

where K_A, K_I are activation and inhibition thresholds for RNA activator rA1 and RNA inhibitor rI2, and the constant $[\mathrm{T}ij^{\mathrm{tot}}]$ is the sum of concentrations of all molecular species containing Tij, that is, the sum of ON-state switch concentration, [TijAj], and OFF-state switch concentration, [Tij]. We then introduce

non-dimensional variables as follows:

$$\begin{aligned} x &= \frac{[\mathrm{rA1}]}{K_A}, \\ y &= \frac{[\mathrm{rI2}]}{K_I}, \\ u &= \frac{[\mathrm{T12A2}]}{[\mathrm{T12^{tot}}]}, \\ v &= \frac{[\mathrm{T21A1}]}{[\mathrm{T21^{tot}}]}, \\ s &= \frac{t}{\tau}. \end{aligned}$$

For instance, starting with

$$\frac{d[\mathrm{rA1}]}{dt} = k_p \cdot [\mathrm{T12A2}] - k_d \cdot [\mathrm{rA1}],$$

by dividing both sides by $k_d \cdot K_A$ and substituting with non-dimensional variables, we obtain

$$\frac{1}{k_d \cdot K_A}\frac{d[\mathrm{rA1}]}{dt} = \frac{1}{k_d \cdot \tau}\frac{dx}{ds} = \frac{k_p[\mathrm{T12^{tot}}]}{k_d \cdot K_A}u - x,$$

and thus,

$$\gamma\frac{dx}{ds} = \alpha \cdot u - x,$$

where $\alpha = \frac{1}{K_A}\frac{k_p}{k_d}[\mathrm{T12^{tot}}]$ and $\gamma = \frac{1}{k_d \cdot \tau}$. Similarly, with $\beta = \frac{1}{K_I}\frac{k_p}{k_d}[\mathrm{T21^{tot}}]$, the other equations are substituted with non-dimensional variables as follows:

$$\begin{aligned} \gamma\frac{dy}{ds} &= \beta \cdot v - y, \\ \frac{du}{ds} &= \frac{1}{1+y^n} - u, \\ \frac{dv}{ds} &= 1 - \frac{1}{1+x^m} - v. \end{aligned}$$

The nullclines for x and y are calculated by letting $\frac{du}{ds} = 0$ and $\frac{dv}{ds} = 0$. At steady-states, $u = \frac{1}{1+y^n}$ and $v = 1 - \frac{1}{1+x^m}$. Thus, a nullcline for x (ie, $\frac{dx}{ds} = 0$) becomes $x = \alpha u = \frac{\alpha}{1+y^n}$ and a nullcline for y (ie, $\frac{dy}{ds} = 0$) becomes $y = \beta\left(1 - \frac{1}{1+x^m}\right)$. The steady-states are where nullclines for x and y intersect. The jacobian matrix J is

$$J = \begin{pmatrix} -\frac{1}{\gamma} & 0 & \frac{\alpha}{\gamma} & 0 \\ 0 & -\frac{1}{\gamma} & 0 & \frac{\beta}{\gamma} \\ 0 & -\frac{ny^{n-1}}{(1+y^n)^2} & -1 & 0 \\ \frac{mx^{m-1}}{(1+x^m)^2} & 0 & 0 & -1 \end{pmatrix}$$

and the characteristic equation of the system is

$$\det(J - \lambda I) = \left(\lambda + \frac{1}{\gamma}\right)^2(\lambda+1)^2 + \frac{\alpha\beta}{\gamma^2}\frac{mx^{m-1}}{(1+x^m)^2}\frac{ny^{n-1}}{(1+y^n)^2} = 0.$$

The stability of steady-states are numerically solved by inspecting the real parts of eigenvalues from the characteristic equations.

Roughly mapping experimental results to the phase diagram of the simple model is performed as follows:

$$\begin{aligned}
\alpha &= \frac{1}{K_A}\frac{k_p}{k_d}[\mathrm{T12^{tot}}] \simeq \frac{\frac{1}{2}\frac{k_{cat,ON,12}}{K_{M,ON,12}}[\mathrm{RNAP}]}{\frac{1}{2}\frac{k_{cat,H,1}}{K_{M,H,1}}[\mathrm{RNaseH}]} \cdot \frac{[\mathrm{T12^{tot}}]}{[\mathrm{dI1^{tot}}] - [\mathrm{A1^{tot}}] + \frac{1}{2}[\mathrm{T21^{tot}}]}, \\
\beta &= \frac{1}{K_I}\frac{k_p}{k_d}[\mathrm{T21^{tot}}] \simeq \frac{\frac{1}{2}\frac{k_{cat,ON,21}}{K_{M,ON,21}}[\mathrm{RNAP}]}{\frac{1}{2}\frac{k_{cat,H,2}}{K_{M,H,2}}[\mathrm{RNaseH}]} \cdot \frac{[\mathrm{T21^{tot}}]}{[\mathrm{A2^{tot}}] - \frac{1}{2}[\mathrm{T12^{tot}}]}, \\
\gamma &= \frac{1}{k_d \cdot \tau} \simeq \frac{4}{\left(\frac{k_{cat,H,1}}{K_{M,H,1}} + \frac{k_{cat,H,2}}{K_{M,H,2}}\right)[\mathrm{RNaseH}]} \cdot \frac{1}{\frac{1}{k[\mathrm{T12^{tot}}]} + \frac{1}{k[\mathrm{T21^{tot}}]}}, \\
n &\simeq 4\frac{K_I}{[\mathrm{T12^{tot}}]} = 4\frac{[\mathrm{A2^{tot}}] - \frac{1}{2}[\mathrm{T12^{tot}}]}{[\mathrm{T12^{tot}}]}, \\
m &\simeq 4\frac{K_A}{[\mathrm{T21^{tot}}]} = 4\frac{[\mathrm{dI1^{tot}}] - [\mathrm{A1^{tot}}] + \frac{1}{2}[\mathrm{T21^{tot}}]}{[\mathrm{T21^{tot}}]},
\end{aligned}$$

where by $\simeq$ we mean that we expect correlations with unitless parameters on the left and formulations of rate constants and concentrations on the right. For instance, $k_{cat,ON,ij}$ and $K_{M,ON,ij}$ are catalytic and Michaelis constants for RNAP, and since the enzyme rates reach half-max speed (ie, $\frac{1}{2}k_{cat,ON,ij} \cdot [\mathrm{RNAP}]$) when the substrate concentration is at its Michaelis constant $K_{M,ON,ij}$, the first-order rate constant k_p is approximately $\frac{1}{2}\frac{k_{cat,ON,ij}}{K_{M,ON,ij}} \cdot [\mathrm{RNAP}]$ for TijAj. Similarly, k_d is approximately $\frac{1}{2}\frac{k_{cat,H,i}}{K_{M,H,i}} \cdot [\mathrm{RNaseH}]$ for RNA signals. To approximate switching thresholds K_A and K_I, and the steepness of such switch responses

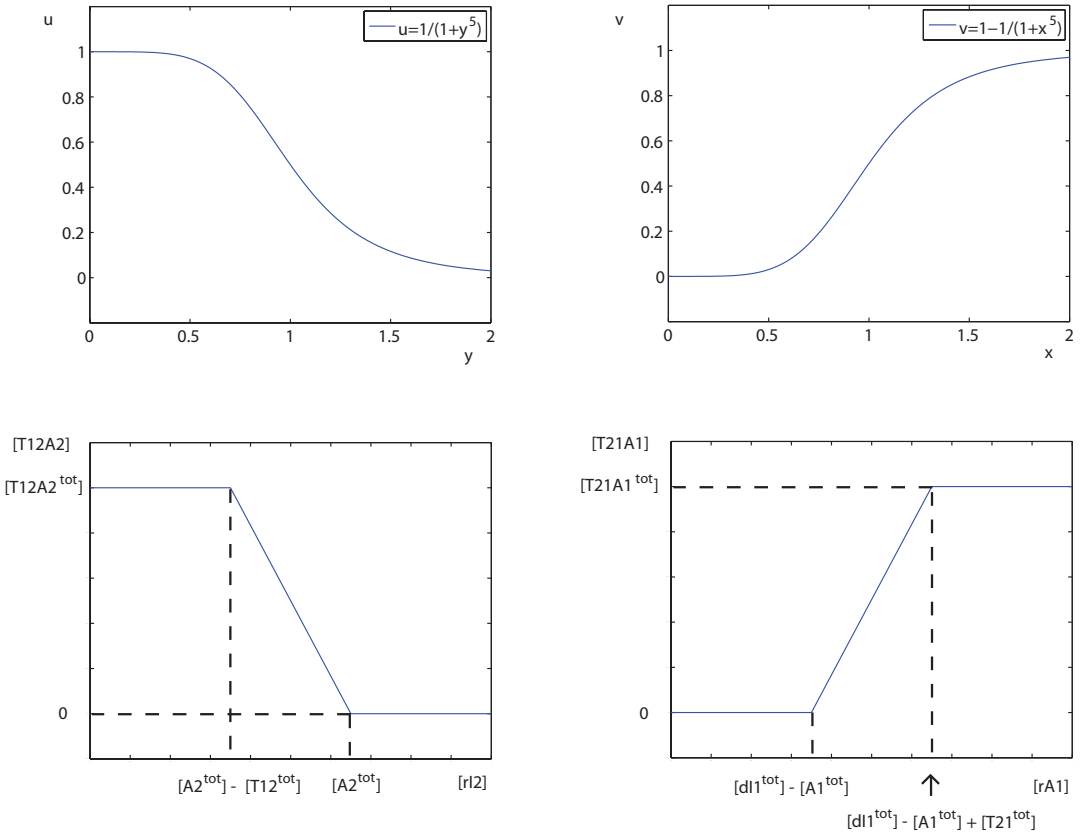

captured by Hill exponents n and m, we use a piece-wise linear graph resulting from assuming completion of hybridization of DNA and RNA species as shown above. The upper left graph shows the steady-state of u as a function of y (ie, $\frac{du}{ds} = 0$) with $n = 5$. The bottom left is the corresponding graph for DNA and RNA species involved. As the input RNA inhibitor rI2 concentration increases, the free

DNA activator A2 in solution binds to rI2 and no change in switch state is apparent until all free A2 is consumed (ie, $[\mathrm{rI2}] = [\mathrm{A2^{tot}}] - [\mathrm{T12^{tot}}]$). After that point, rI2 can displace A2 from the T12A2 complex in stoichiometric amounts until all A2 is displaced when the total concentrations of rI2 and A2 coincide (ie, $[\mathrm{rI2}] = [\mathrm{A2^{tot}}]$). Thus, the inhibition threshold K_I corresponds to the point where the switch T12 is half ON: $K_I \simeq [\mathrm{A2^{tot}}] - \frac{1}{2}[\mathrm{T12^{tot}}]$. At the switching threshold, the slope is $-\frac{n}{4}$ for the y vs u graph ($\frac{du}{dy}|_{y=1} = -\frac{ny^{n-1}}{(1+y^n)^2}|_{y=1} = -\frac{n}{4}$). The slope is -1 for the [T12A2] vs [rI2] graph at the switching threshold, which corresponds to a slope of $-\frac{K_I}{[\mathrm{T12^{tot}}]}$ for the $u = \frac{[\mathrm{T12A2}]}{[\mathrm{T12^{tot}}]}$ vs $y = \frac{[\mathrm{rI2}]}{K_I}$ graph. Thus, we derived the above relation: $n \simeq 4\frac{K_I}{[\mathrm{T12^{tot}}]}$. Similarly, using the piece-wise linear approximation for rA1 and switch T21, $K_A \simeq [\mathrm{dI1^{tot}}] - [\mathrm{A1^{tot}}] + \frac{1}{2}[\mathrm{T21^{tot}}]$ and $m \simeq 4\frac{K_A}{[\mathrm{T21^{tot}}]}$. The piece-wise linear approximation is less accurate for RNA inputs than for DNA inputs due to constant turn over of RNA species by enzymes (2). However, the steepness would be correlated with the relative concentrations of DNA and RNA species.

We also calculate the time-scale of hybridization reaction near steady-states to approximate τ. Let's consider the following reaction with a bimolecular hybridization rate k:

$$\mathrm{T12} + \mathrm{A2} \quad \xrightarrow{\quad k \quad} \quad \mathrm{T12A2}.$$

Then, the reaction rates are simply $\frac{d[\mathrm{T12A2}]}{dt} = k[\mathrm{T12}][\mathrm{A2}]$. Using the piece-wise linear approximation above, we first assume that at steady-state $[\mathrm{T12}] \approx [\mathrm{T12A2}] \approx \frac{[\mathrm{T12^{tot}}]}{2}$ and $[\mathrm{A2}] \approx 0$. Any perturbation of the steady-state by additional A2, provided by RNase H mediated degradation of the A2·rI2 complex, can shift steady-state of T12A2 by the same amount until the freely available A2 approaches zero again. That is, the new steady-state of T12A2 is approximately the sum of current T12A2 concentration and A2 concentration $\left([\mathrm{T12^{tot}}]\frac{1}{1+\left(\frac{[\mathrm{rI2}]}{K_I}\right)^n} \simeq [\mathrm{T12A2}] + [\mathrm{A2}]\right)$. Thus, $\frac{d[\mathrm{T12A2}]}{dt} \approx k[\mathrm{T12}][\mathrm{A2}] \simeq \frac{1}{\tau}[\mathrm{A2}]$, and we derive the approximation $\frac{1}{\tau} \simeq \frac{k[\mathrm{T12^{tot}}]}{2}$. We assume that other hybridization and toehold-mediated branch migration rates involving switch templates are similar. Then, $\tau \simeq \frac{2}{k[\mathrm{T}ij^{\mathrm{tot}}]}$. We use the averages of k_d and τ for the two switches to approximate γ.

Although the biochemical rate constants (e.g. k_{cat} and K_M) are not explicitly known and must be fit to experimental results, if we take ratios of these unitless parameters for different experiments, they are independent of these rate constants. Thus, we chose somewhat arbitrarily reaction #20 as the default reaction for those using enzyme batch #1 and reaction #37 as the default reaction for those using enzyme batch #2 with $\alpha_0 = 1.7, \beta_0 = 1.7, \gamma_0 = 1, n_0 = 5, m_0 = 5$. The values for other reactions, say reaction r, are determined as follows:

$$\begin{aligned}
\alpha_r &= \alpha_0 \left(\frac{[\mathrm{RNAP}]}{[\mathrm{RNaseH}]} \cdot \frac{[\mathrm{T12^{tot}}]}{[\mathrm{dI1^{tot}}] - [\mathrm{A1^{tot}}] + \frac{1}{2}[\mathrm{T21^{tot}}]}\right) \Big/ \left(\frac{[\mathrm{RNAP}]_0}{[\mathrm{RNaseH}]_0} \cdot \frac{[\mathrm{T12^{tot}}]_0}{[\mathrm{dI1^{tot}}]_0 - [\mathrm{A1^{tot}}]_0 + \frac{1}{2}[\mathrm{T21^{tot}}]_0}\right), \\
\beta_r &= \beta_0 \left(\frac{[\mathrm{RNAP}]}{[\mathrm{RNaseH}]} \cdot \frac{[\mathrm{T21^{tot}}]}{[\mathrm{A2^{tot}}] - \frac{1}{2}[\mathrm{T12^{tot}}]}\right) \Big/ \left(\frac{[\mathrm{RNAP}]_0}{[\mathrm{RNaseH}]_0} \cdot \frac{[\mathrm{T21^{tot}}]_0}{[\mathrm{A2^{tot}}]_0 - \frac{1}{2}[\mathrm{T12^{tot}}]_0}\right), \\
\gamma_r &= \gamma_0 \left(\frac{1}{[\mathrm{RNaseH}]} \frac{1}{\frac{1}{[\mathrm{T12^{tot}}]} + \frac{1}{[\mathrm{T21^{tot}}]}}\right) \Big/ \left(\frac{1}{[\mathrm{RNaseH}]_0} \frac{1}{\frac{1}{[\mathrm{T12^{tot}}]_0} + \frac{1}{[\mathrm{T21^{tot}}]_0}}\right), \\
n_r &= n_0 \left(\frac{[\mathrm{A2^{tot}}] - \frac{1}{2}[\mathrm{T12^{tot}}]}{[\mathrm{T12^{tot}}]}\right) \Big/ \left(\frac{[\mathrm{A2^{tot}}]_0 - \frac{1}{2}[\mathrm{T12^{tot}}]_0}{[\mathrm{T12^{tot}}]_0}\right), \\
m_r &= m_0 \left(\frac{[\mathrm{dI1^{tot}}] - [\mathrm{A1^{tot}}] + \frac{1}{2}[\mathrm{T21^{tot}}]}{[\mathrm{T21^{tot}}]}\right) \Big/ \left(\frac{[\mathrm{dI1^{tot}}]_0 - [\mathrm{A1^{tot}}]_0 + \frac{1}{2}[\mathrm{T21^{tot}}]_0}{[\mathrm{T21^{tot}}]_0}\right).
\end{aligned}$$

The phase diagram of simple model was constructed for the α vs β plane, and the m vs n plane, setting other unitless parameters to default values. Using (α_r, β_r) and (m_r, n_r) coordinates, experimental results are

mapped to phase diagram as stable (circles, damping coefficient less than .15/hr, as calculated in section 3), damped (dots, damping coefficient between .15/hr and .5/hr), and strongly damped (crosses, damping coefficient greater than .5/hr) oscillations. This mapping is expected to be unsatisfactory, because in each diagram, the three unitless parameters that are held constant in the simple model calculation actually vary considerably in the estimates for experimental conditions. Indeed, while the experimental measurements

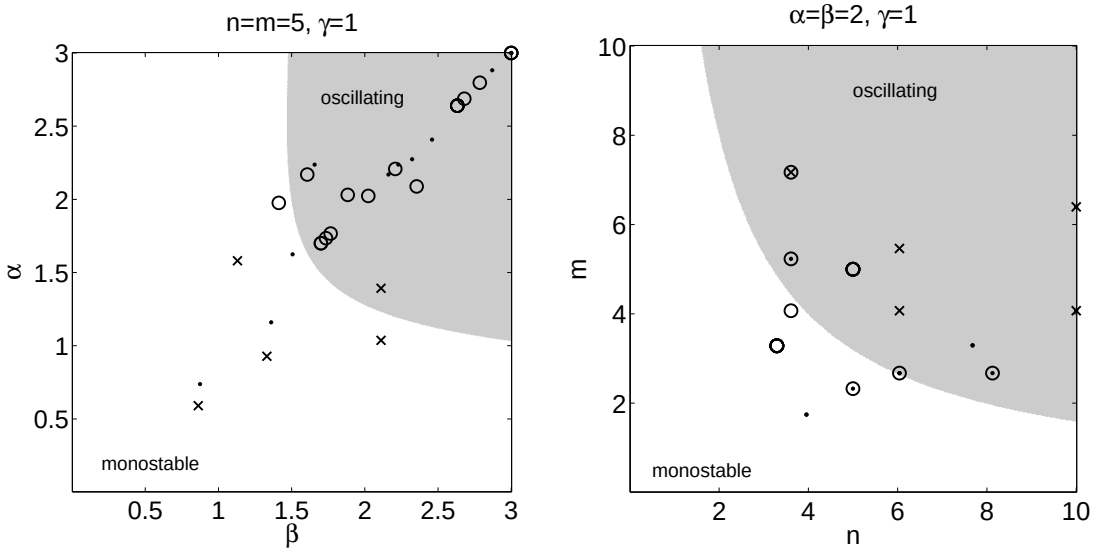

showed some correlation with the simple model phase diagram when considering just α_r and β_r pairs, the experimental measurements did not correlate with phase diagram for m_r and n_r pairs. Note however that these parameters are correlated for certain experimental choice of DNA and enzyme concentrations. For instance, increasing K_I by means of adjusting $[\mathrm{A2^{tot}}]$ would increase n_r but decrease β_r. We observed that experimental conditions corresponding to strongly damped oscillations had higher n_r and m_r values that are permissive for sustained oscillation, yet lower α_r and β_r values that are prohibitive for sustained oscillation. Therefore, we constructed another phase diagram for the α vs n plane, assuming $\alpha = \beta$ and $m = n$ (Figure 2). Since the products $\alpha \cdot \beta$ and $m \cdot n$ appear in the characteristic equations, geometric means of these pairs were reasonable approximations to map experimental results. Using $(\sqrt{\alpha_r \cdot \beta_r},\ \sqrt{m_r \cdot n_r})$ coordinates, experimental results are mapped to α vs n plane as stable (circles), damped (dots), and strongly damped or too slow to measure (crosses) oscillations.

1.1.1 Two-dimensional simple models

Here we consider two limiting cases for time-scale separation, ie, for very large and very small γ.

First, if $\gamma \gg 1$, x and y dynamics become very slow compared to u and v dynamics. Thus, we can assume $\frac{du}{ds} = 0$ and $\frac{dv}{ds} = 0$. Re-scaling time by $\frac{1}{\gamma}$ results in the following non-dimensional equations:

$$\begin{aligned} \frac{dx}{ds} &= \alpha \cdot \frac{1}{1+y^n} - x, \\ \frac{dy}{ds} &= \beta \cdot \left(1 - \frac{1}{1+x^m}\right) - y. \end{aligned}$$

The jacobian matrix J is

$$J = \begin{pmatrix} -1 & -\frac{\alpha n y^{n-1}}{(1+y^n)^2} \\ \frac{\beta m x^{m-1}}{(1+x^m)^2} & -1 \end{pmatrix}.$$

and the characteristic equation of the system is

$$\det(J - \lambda I) = (\lambda + 1)^2 + \frac{\alpha\beta m x^{m-1} n y^{n-1}}{(1+x^m)^2(1+y^n)^2} = 0.$$

Because in the current biochemical equations $x, y \geq 0$, the solution is simply $\lambda = -1 \pm \sqrt{\frac{\alpha\beta m x^{m-1} n y^{n-1}}{(1+x^m)^2(1+y^n)^2}}i$. Hence, the system always has stable steady-states and oscillation is not possible for any combination of α, β, n, and m parameters.

Second, if $\gamma \ll 1$, u and v dynamics become very slow compared to x and y dynamics. Assuming $\frac{dx}{ds} = 0$ and $\frac{dy}{ds} = 0$, we derive the following equations:

$$\begin{aligned} \frac{du}{ds} &= \frac{1}{1+(\beta v)^n} - u, \\ \frac{dv}{ds} &= 1 - \frac{1}{1+(\alpha u)^m} - v. \end{aligned}$$

The jacobian matrix J is

$$J = \begin{pmatrix} -1 & -\frac{\beta^n n v^{n-1}}{(1+(\beta v)^n)^2} \\ \frac{\alpha^m m u^{m-1}}{(1+(\alpha u)^m)^2} & -1 \end{pmatrix}.$$

and the characteristic equation of the system is

$$\det(J - \lambda I) = (\lambda+1)^2 + \frac{\alpha^m m u^{m-1}}{(1+(\alpha u)^m)^2} \cdot \frac{\beta^n n v^{n-1}}{(1+(\beta v)^n)^2} = 0.$$

Since $u, v \geq 0$, the solution is simply $\lambda = -1 \pm \sqrt{\frac{\alpha^m m u^{m-1}}{(1+(\alpha u)^m)^2} \cdot \frac{\beta^n n v^{n-1}}{(1+(\beta v)^n)^2}}i$. Therefore, for both limiting cases, the system has stable steady-states and oscillation is not allowed.

In fact, similar arguments prohibit oscillation in any two dimensional dynamical system of the form $\frac{dx}{ds} = f_1(y) - f_2(x)$, $\frac{dy}{ds} = g_1(x) - f_3(y)$, where f_1, f_2, and f_3 are monotonic, positive, and increasing, and g_1 is monotonic, positive, and decreasing. In that case, the jacobian is

$$J = \begin{pmatrix} -a & b \\ -c & -d \end{pmatrix}$$

where $a, b, c, d > 0$, and thus there is no eigenvalue with positive real part. Therefore, to observe oscillations, we need either a delay (which we effectively introduced by considering 4-dimensional dynamics) or more complex interactions (such as non-monotonic coupling due to Michaelis-Menten saturation of enzymes).

1.2 A simple model of the amplified negative feedback oscillator (Design II)

For the Design II oscillator we introduce a new switch T11 in addition to the components of the Design I oscillator:

$$\begin{aligned} \frac{d[\mathrm{rA1}]}{dt} &= k_p \cdot [\mathrm{T12A2}] + k_p \cdot [\mathrm{T11A1}] - k_d \cdot [\mathrm{rA1}], \\ \frac{d[\mathrm{rI2}]}{dt} &= k_p \cdot [\mathrm{T21A1}] - k_d \cdot [\mathrm{rI2}], \\ \frac{d[\mathrm{T12A2}]}{dt} &= \frac{1}{\tau}\left([\mathrm{T12^{tot}}] \frac{1}{1+\left(\frac{[\mathrm{rI2}]}{K_I}\right)^n} - [\mathrm{T12A2}] \right), \\ \frac{d[\mathrm{T21A1}]}{dt} &= \frac{1}{\tau}\left([\mathrm{T21^{tot}}] \left(1 - \frac{1}{1+\left(\frac{[\mathrm{rA1}]}{K_A}\right)^m}\right) - [\mathrm{T21A1}] \right), \\ \frac{d[\mathrm{T11A1}]}{dt} &= \frac{1}{\tau}\left([\mathrm{T11^{tot}}] \left(1 - \frac{1}{1+\left(\frac{[\mathrm{rA1}]}{K_A}\right)^m}\right) - [\mathrm{T11A1}] \right). \end{aligned}$$

Using non-dimensional parameter $w = \frac{[\mathrm{T11A1}]}{[\mathrm{T11^{tot}}]}$ and letting $\delta = \frac{1}{K_A}\frac{k_p}{k_d}[\mathrm{T11^{tot}}]$,

$$\begin{aligned}
\gamma\frac{dx}{ds} &= \alpha \cdot u + \delta \cdot w - x, \\
\gamma\frac{dy}{ds} &= \beta \cdot v - y, \\
\frac{du}{ds} &= \frac{1}{1+y^n} - u, \\
\frac{dv}{ds} &= 1 - \frac{1}{1+x^m} - v, \\
\frac{dw}{ds} &= 1 - \frac{1}{1+x^m} - w.
\end{aligned}$$

The nullclines for x and y are calculated by letting $\frac{du}{ds} = 0$, $\frac{dv}{ds} = 0$, and $\frac{dw}{ds} = 0$. At steady-states, $u = \frac{1}{1+y^n}$ and $v = w = 1 - \frac{1}{1+x^m}$. Thus, a nullcline for x (ie, $\frac{dx}{ds} = 0$) becomes $x = \alpha u + \delta w = \frac{\alpha}{1+y^n} + \delta\left(1 - \frac{1}{1+x^m}\right)$ and a nullcline for y (ie, $\frac{dy}{ds} = 0$) becomes $y = \beta\left(1 - \frac{1}{1+x^m}\right)$. The steady-states are where nullclines for x and y intersect. For simplicity, if we assume that the initial conditions for v and w are identical (ie, $v(s=0) = w(s=0)$), the trajectories for v and w remain identical. Thus, we assume $v = w$, and exclude w from stability analysis. Without w, the jacobian matrix J is

$$J = \begin{pmatrix}
-\frac{1}{\gamma} & 0 & \frac{\alpha}{\gamma} & \frac{\delta}{\gamma} \\
0 & -\frac{1}{\gamma} & 0 & \frac{\beta}{\gamma} \\
0 & -\frac{ny^{n-1}}{(1+y^n)^2} & -1 & 0 \\
\frac{mx^{m-1}}{(1+x^m)^2} & 0 & 0 & -1
\end{pmatrix}$$

and the characteristic equation of the system is

$$\det(J - \lambda I) = \left(\lambda + \frac{1}{\gamma}\right)^2 (\lambda+1)^2 + \frac{\alpha\beta}{\gamma^2}\frac{mx^{m-1}}{(1+x^m)^2}\frac{ny^{n-1}}{(1+y^n)^2} - \frac{\delta}{\gamma}\left(\lambda + \frac{1}{\gamma}\right)(\lambda+1)\frac{mx^{m-1}}{(1+x^m)^2} = 0.$$

Mapping experimental results to the phase diagram of simple model is performed as before. We chose reaction #37 of the two-switch negative feedback oscillator as the default reaction with $\alpha_0 = 1.7, \beta_0 = 1.7, \gamma_0 = 1, n_0 = 5, m_0 = 5$. The values for other reactions are determined as described earlier for $\alpha_r, \beta_r, \gamma_r, n_r$, and m_r. In addition, δ_r is calculated as follows:

$$\delta_r = \alpha_r \frac{[\mathrm{T11^{tot}}]}{[\mathrm{T12^{tot}}]}.$$

The results are shown for the α vs δ plane (Figure 4). Using (α_r, δ_r) coordinates, experimental results are mapped to α vs δ plane as stable (circles), and strongly damped or too slow to measure (crosses) oscillations. Regimes within the phase plane are defined by the number and stability pattern of the steady states. For example, the oscillating regime is (+), the monostable regimes are (-), the bistable regime is (-,+,-), as indicated in Figure 4. More intricate behaviors are observed near the intersection of the monostable, bistable, and oscillating regimes.

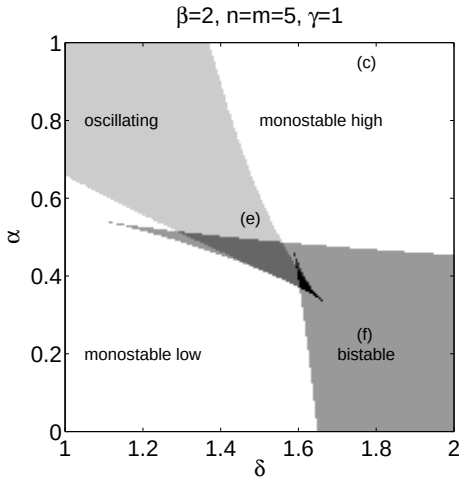

For example, there is the oscillating/stable regime with three steady-states and a stability pattern of (-,+,+) (dark grey area below (e)), as well as regimes with five steady-states and stability patterns of (-,+,-,+,-) (darker grey area above black area) and (-,+,+,+,-) (black area). Example phase portraits in the oscillating/stable regime and in the regimes with five steady-states are shown below.

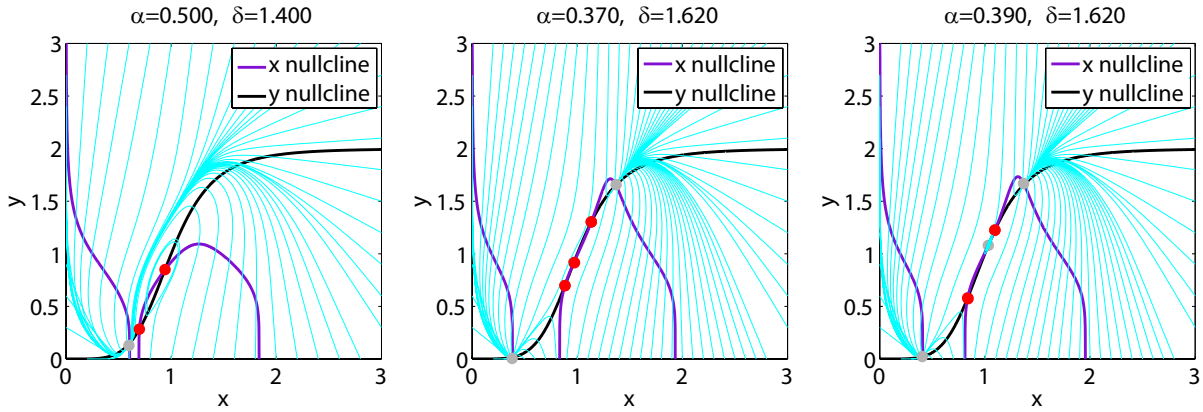

Interestingly, a phase portrait similar to that of a relaxation oscillator – an oscillator that possesses a bistable trigger (3), whereby the system is driven around the hysteresis loop (4) – was observed within the oscillating regime near the oscillating/stable regime, with $\alpha = 0.5$ and $\delta = 1.5$, marked (e). The additional positive feedback loop puts a kink in the x nullcline such that x becomes bistable for y values close to its fixed point, providing the basis for relaxation oscillator behavior. The corresponding x-y phase portrait and time-courses of non-dimensional variables are shown below.

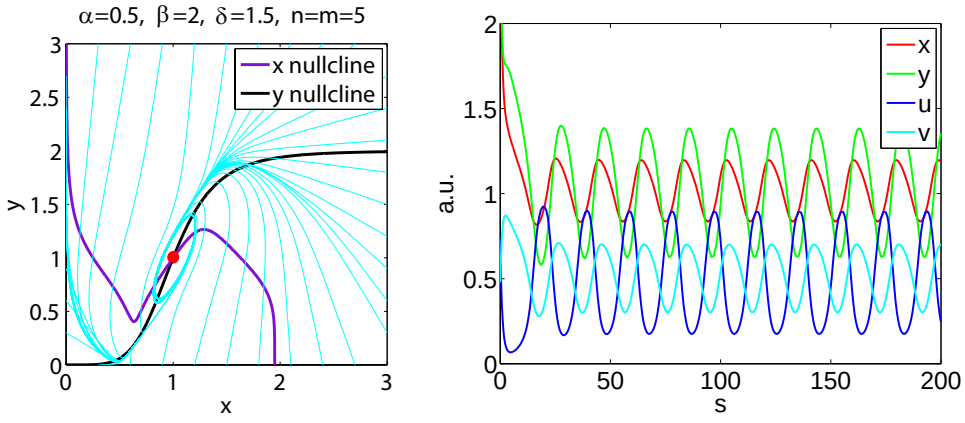

However, the characteristic spike-like oscillations associated with relaxation oscillators were not present with these parameter choices. If there were a time-scale separation where y changes much slower than x, we would expect typical relaxation oscillator behavior to result. That not being an option in this simple model (although modifications of the experimental system could be considered), we explored the phase space at different cross-sections of β and n values, and found more clear relaxation oscillator behavior as shown below. The following x-y phaseplane and time-courses are plotted with $\alpha = 0.57$, $\beta = 2.5$, $\delta = 1.5$, and $n = 6.5$.

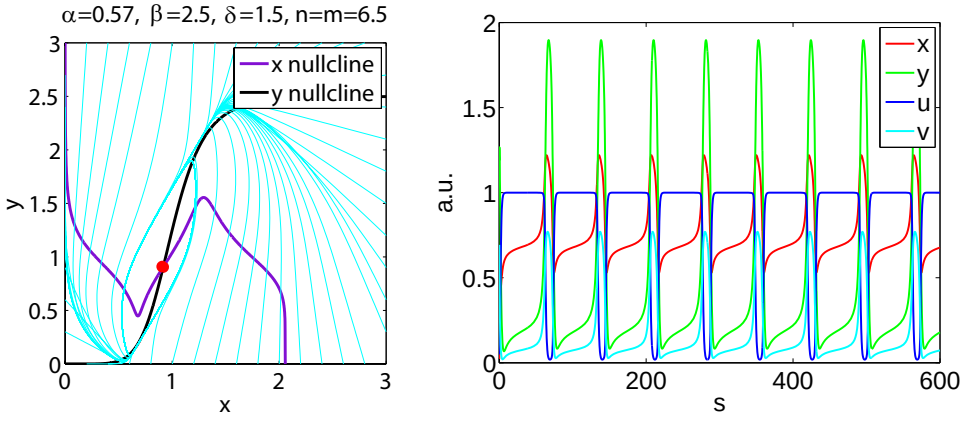

1.3 A simple model of the three-switch ring oscillator (Design III)

For the Design III oscillator, we take the three RNA species as dynamic signals and assume that their production rates are solely determined by the ON-state switch concentrations and their degradation rates depend only on their own concentrations. Unlike the other simple models for Design I and II oscillators, for simplicity here our simple model assumes that the ON-state switches equilibrate instantly with changing RNA inhibitor concentrations. On the other hand, the degradation rates saturate with high RNA concentrations, mimicking the saturation of RNase H that mediates the degradation processes.

$$\begin{aligned}
\frac{d[\mathrm{rI1}]}{dt} &= k_p[\mathrm{T12A2}] - v_d\frac{[\mathrm{rI1}]}{K_d + [\mathrm{rI1}]} \\
&= k_p[\mathrm{T12}^{\mathrm{tot}}]\frac{1}{1+\left(\frac{[\mathrm{rI2}]}{K_I}\right)^n} - v_d\frac{[\mathrm{rI1}]}{K_d + [\mathrm{rI1}]}, \\
\frac{d[\mathrm{rI2}]}{dt} &= k_p[\mathrm{T23}^{\mathrm{tot}}]\frac{1}{1+\left(\frac{[\mathrm{rI3}]}{K_I}\right)^n} - v_d\frac{[\mathrm{rI2}]}{K_d + [\mathrm{rI2}]}, \\
\frac{d[\mathrm{rI3}]}{dt} &= k_p[\mathrm{T31}^{\mathrm{tot}}]\frac{1}{1+\left(\frac{[\mathrm{rI1}]}{K_I}\right)^n} - v_d\frac{[\mathrm{rI3}]}{K_d + [\mathrm{rI3}]},
\end{aligned}$$

where k_p is the production rate from an ON-state switch, K_I is the inhibition threshold similar to other models, v_d is the maximum degradation rate (ie, $k_{cat,H}[\mathrm{RNaseH}]$), and K_d is the Michaelis constant for RNase H saturation. With $(i, j) \in \{(1, 2), (2, 3), (3, 1)\}$, the above equations become

$$\frac{d[\mathrm{rI}i]}{dt} = k_p[\mathrm{T}ij^{\mathrm{tot}}]\frac{1}{1+\left(\frac{[\mathrm{rI}j]}{K_I}\right)^n} - v_d\frac{[\mathrm{rI}i]}{K_d + [\mathrm{rI}i]}.$$

We then introduce non-dimensional variables as follows:

$$\begin{aligned} x_i &= \frac{[\mathrm{rI}i]}{K_I}, \\ s &= t\frac{v_d}{K_I}. \end{aligned}$$

Dividing both sides by v_d and substituting with non-dimensional variables,

$$\frac{K_I}{v_d}\frac{d}{dt}\frac{[\mathrm{rI}i]}{K_I} = \frac{dx_i}{ds} = \frac{k_p}{v_d}[\mathrm{T}ij^{\mathrm{tot}}]\frac{1}{1+x_j^n} - \left(1 - \frac{1}{1+\frac{K_I}{K_d}x_i}\right),$$

thus,

$$\frac{dx_i}{ds} = \alpha\frac{1}{1+x_j^n} - \left(1 - \frac{1}{1+\frac{x_i}{\beta}}\right),$$

with $\alpha = \frac{k_p}{v_d}[\mathrm{T}ij^{\mathrm{tot}}]$ and $\beta = \frac{K_d}{K_I}$, assuming that all $[\mathrm{T}ij^{\mathrm{tot}}]$ are identical.

The jacobian matrix J is

$$J = \begin{pmatrix} -\frac{1}{\beta\left(1+\frac{x_1}{\beta}\right)^2} & -\alpha\frac{nx_2^{n-1}}{(1+x_2^n)^2} & 0 \\ 0 & -\frac{1}{\beta\left(1+\frac{x_2}{\beta}\right)^2} & -\alpha\frac{nx_3^{n-1}}{(1+x_3^n)^2} \\ -\alpha\frac{nx_1^{n-1}}{(1+x_1^n)^2} & 0 & -\frac{1}{\beta\left(1+\frac{x_3}{\beta}\right)^2} \end{pmatrix}$$

and the characteristic equation of the system is

$$\det(J-\lambda I) = \left(\lambda + \frac{1}{\beta\left(1+\frac{x_{ss}}{\beta}\right)^2}\right)^3 + \left(\frac{\alpha n x_{ss}^{n-1}}{(1+x_{ss}^n)^2}\right)^3 = 0,$$

where the system is at steady-state $x_1 = x_2 = x_3 = x_{ss}$. The stability of steady-states are numerically solved by inspecting the real parts of eigenvalues from the characteristic equations.

Roughly mapping experimental results to the phase diagram of the simple model is performed similar to previous cases as follows:

$$\begin{aligned} \alpha &= \frac{k_p}{v_d}[\mathrm{T}ij^{\mathrm{tot}}] \simeq \frac{\frac{1}{2}\frac{k_{cat,ON}}{K_{M,ON}}[\mathrm{RNAP}][\mathrm{T}ij^{\mathrm{tot}}]}{k_{cat,H}[\mathrm{RNaseH}]}, \\ \beta &= \frac{K_d}{K_I} \simeq \frac{K_{M,H}}{[\mathrm{A}j^{\mathrm{tot}}] - \frac{1}{2}[\mathrm{T}ij^{\mathrm{tot}}]}, \\ n &\simeq 4\frac{K_I}{[\mathrm{T}ij^{\mathrm{tot}}]} = 4\frac{[\mathrm{A}j^{\mathrm{tot}}] - \frac{1}{2}[\mathrm{T}ij^{\mathrm{tot}}]}{[\mathrm{T}ij^{\mathrm{tot}}]}, \end{aligned}$$

where $k_{cat,ON}$ is the catalytic rate of RNAP for ON-state switch, $K_{M,ON}$ is the Michaelis constant of RNAP for ON-state switch, $k_{cat,H}$ is the catalytic rate of RNase H, and $K_{M,H}$ is the Michaelis constant of RNase H. We chose reaction #27 as the default reaction with $\alpha_0 = 1.7, \beta_0 = 0.3, n_0 = 3.5$. The values for other reactions are determined as follows using the geometric mean for DNA concentrations (since in the

experiments, the three switches were not symmetric):

$$\begin{aligned}
\alpha_r &= \alpha_0 \left(\frac{[\mathrm{RNAP}]}{[\mathrm{RNaseH}]} \cdot (\prod_{i,j} [\mathrm{T}ij^{\mathrm{tot}}])^{\frac{1}{3}} \right) / \left(\frac{[\mathrm{RNAP}]_0}{[\mathrm{RNaseH}]_0} \cdot (\prod_{i,j} [\mathrm{T}ij^{\mathrm{tot}}]_0)^{\frac{1}{3}} \right), \\
\beta_r &= \beta_0 \left(\prod_{i,j} \frac{[\mathrm{A}j^{\mathrm{tot}}]_0 - \frac{1}{2}[\mathrm{T}ij^{\mathrm{tot}}]_0}{[\mathrm{A}j^{\mathrm{tot}}] - \frac{1}{2}[\mathrm{T}ij^{\mathrm{tot}}]} \right)^{\frac{1}{3}}, \\
n_r &= n_0 \left(\prod_{i,j} \frac{[\mathrm{A}j^{\mathrm{tot}}] - \frac{1}{2}[\mathrm{T}ij^{\mathrm{tot}}]}{[\mathrm{A}j^{\mathrm{tot}}]_0 - \frac{1}{2}[\mathrm{T}ij^{\mathrm{tot}}]_0} \cdot \frac{[\mathrm{T}ij^{\mathrm{tot}}]_0}{[\mathrm{T}ij^{\mathrm{tot}}]} \right)^{\frac{1}{3}}.
\end{aligned}$$

The results are shown for the α vs n plane (Figure 6) and for the α vs β plane. Because the simple

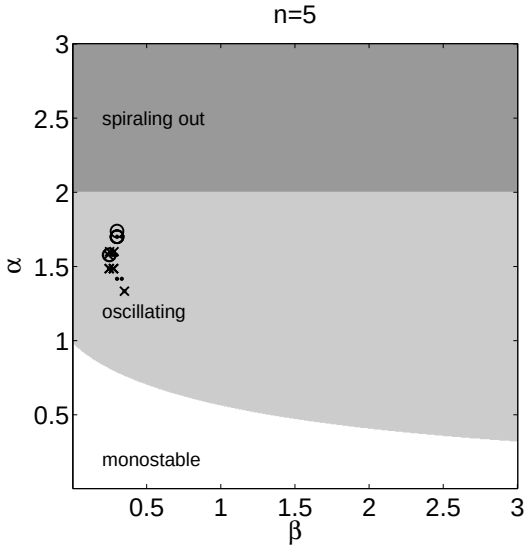

model has a degradation function that saturates with increasing substrate concentration, with a maximum degradation rate of 1, in addition to limit oscillations we observed a qualitatively different behavior in the phase diagram, marked as 'spiraling out'. During 'spiraling out' behavior, the sum of x_is (that is, the sum of the concentrations of RNA inhibitor species) may grow without bound for some initial conditions. Note that for some parameters, the 'spiraling out' behavior can coexist with a stable limit oscillation or a stable steady-state, and which behavior occurs depends on initial conditions.

To determine when 'spiraling out' is possible, we consider an initial condition with arbitrarily large initial concentrations in the cycle: one very small, one large and increasing, one large but decreasing. Let $f(x)$ be

$$f(x) = \alpha \frac{1}{1+x^n} - \left(1 - \frac{1}{1+\frac{x}{\beta}}\right),$$

then,

$$f(x_1) + f(x_2) + f(x_3) = \frac{dx_1}{ds} + \frac{dx_2}{ds} + \frac{dx_3}{ds}.$$

Note that

$$\frac{f(x)}{dx} = -\alpha \frac{n x^{n-1}}{(1+x^n)^2} - \frac{1}{\beta \left(1+\frac{x}{\beta}\right)^2} < 0 \quad \text{for} \quad x > 0,$$

such that $f(x)$ has its maximum $f(0) = \alpha$ at $x = 0$ and minimum $f(\infty) = -1$ at $x = \infty$. As long as one of the x_is remain close to 0 during the reaction, the overall growth rate for the sum of all three species become positive for $\alpha > 2$ since $f(x_1) + f(x_2) + f(x_3) \approx f(0) + 2f(\infty) = \alpha - 2$.

More specifically, assume that $\alpha > 2$ and the initial condition is $x_1 = A_0 \gg 1$, $x_2 = 0$, and $x_3 = A_0$, then $\dot{x_1} \approx \alpha - 1$, $\dot{x_2} \approx 0$, and $\dot{x_3} \approx -1$. That is, the system is at a point where a large decreasing signal meets a large increasing signal, and the third signal is pulled low. The derivatives stay roughly the same until x_3 reduces to a very low level after about A_0 time steps. Then, we expect $x_1 \approx A_0\alpha$, $x_2 \approx 0$, and $x_3 \approx 0$. At this point, the derivatives change, as x_3 is no longer sufficient to suppress production of x_2, and we have $\dot{x_1} \approx -1$, $\dot{x_2} \approx \alpha - 1$, and $\dot{x_3} \approx 0$. This continues until after another A_0 time steps, x_1 and x_2 meet at $A_0(\alpha - 1)$, completing the cycle. The cycle continues in this fashion (c.f. Figure 6). Hence, it is possible that the system can show 'spiraling out' behavior if $\alpha > 2$.

While this informal argument captures the essence of the behavior for $n > 1$, we must be careful to show that this informal argument yields the correct result for all n, even $n \ll 1$, where x must be extremely close to zero before $f(x)$ approaches its maximum. We explicitly demonstrate the sufficiency of a large enough initial condition: $x_1 = A_0$, $x_3 = A_0$, and $x_2 < \epsilon = \sqrt[n]{\alpha/2 - 1}$. First note that $\frac{dx_1}{ds} = \alpha\frac{1}{1+x_2^n} - \left(1 - \frac{1}{1+\frac{x_1}{\beta}}\right) > 1$, so x_1 increases faster than x_3 can possibly decrease. Second, we require that x_2 will remain sufficiently small for arbitrarily long while x_1 and x_3 are large and trade off against each other. Since for small x_2, we have $\frac{dx_2}{ds} \approx \alpha\frac{1}{1+x_3^n} - x_2/\beta$, under these conditions $x_2 \to \beta\alpha\frac{1}{1+x_3^n}$. Thus, x_2 remains small enough if $\beta\alpha\frac{1}{1+x_3^n} < \sqrt[n]{\alpha/2 - 1}$, which is true for $1 + x_3^n > \beta\alpha/\epsilon$. A_0 can be chosen sufficiently large to make this true; for larger A_0, the 'trade-off' period can be made arbitrarily large, and dominates the behavior. Thus, the 'spiraling out' behavior is possible for any $n > 0$. We verified this analysis with numerical simulation for a wide range of β and n.

The simple model does not capture all the characteristics of experimental results, at least in part due to the asymmetry among the three switches. However, the simple model does capture the qualitatively different regimes of behavior, including a spiraling-out oscillation rather than a limit-cycle oscillation for some parameters and initial conditions.

1.4 A detailed model of the two-switch negative feedback oscillator (Design I)

A detailed model for DNA and RNA hybridization reactions, branch migration reactions, and Michaelis–Menten enzyme reactions for the Design I oscillator is as follows. Figure 1 shows the four types of hybridization and branch migration reactions.

DNA/RNA hybridization and branch migration reactions

$$
\begin{aligned}
\mathrm{T12} + \mathrm{A2} &\xrightarrow{k_{TA,12}} \mathrm{T12A2} && \text{(Activation)},\\
\mathrm{T21} + \mathrm{A1} &\xrightarrow{k_{TA,21}} \mathrm{T21A1} && \text{(Activation)},\\
\mathrm{A1} + \mathrm{dI1} &\xrightarrow{k_{AI,1}} \mathrm{A1dI1} && \text{(Annihilation)},\\
\mathrm{rA1} + \mathrm{dI1} &\xrightarrow{k_{rAI,1}} \mathrm{rA1dI1} && \text{(Annihilation)},\\
\mathrm{A2} + \mathrm{rI2} &\xrightarrow{k_{AI,2}} \mathrm{A2rI2} && \text{(Annihilation)},\\
\mathrm{T12A2} + \mathrm{rI2} &\xrightarrow{k_{TAI,12}} \mathrm{T12} + \mathrm{A2rI2} && \text{(Inhibition)},\\
\mathrm{T21A1} + \mathrm{dI1} &\xrightarrow{k_{TAI,21}} \mathrm{T21} + \mathrm{A1dI1} && \text{(Inhibition)},\\
\mathrm{rA1} + \mathrm{A1dI1} &\xrightarrow{k_{AIrA,1}} \mathrm{rA1dI1} + \mathrm{A1} && \text{(Release)}.
\end{aligned}
$$

Michaelis–Menten enzyme reactions

$$
\begin{aligned}
\mathrm{RNAP} + \mathrm{T12A2} &\underset{k_{-,ON,12}}{\overset{k_+}{\rightleftharpoons}} \mathrm{RNAP}\cdot\mathrm{T12A2} \xrightarrow{k_{cat,ON,12}} \mathrm{RNAP} + \mathrm{T12A2} + \mathrm{rA1},\\
\mathrm{RNAP} + \mathrm{T21A1} &\underset{k_{-,ON,21}}{\overset{k_+}{\rightleftharpoons}} \mathrm{RNAP}\cdot\mathrm{T21A1} \xrightarrow{k_{cat,ON,21}} \mathrm{RNAP} + \mathrm{T21A1} + \mathrm{rI2},\\
\mathrm{RNAP} + \mathrm{T12} &\underset{k_{-,OFF,12}}{\overset{k_+}{\rightleftharpoons}} \mathrm{RNAP}\cdot\mathrm{T12} \xrightarrow{k_{cat,OFF,12}} \mathrm{RNAP} + \mathrm{T12} + \mathrm{rA1},\\
\mathrm{RNAP} + \mathrm{T21} &\underset{k_{-,OFF,21}}{\overset{k_+}{\rightleftharpoons}} \mathrm{RNAP}\cdot\mathrm{T21} \xrightarrow{k_{cat,OFF,21}} \mathrm{RNAP} + \mathrm{T21} + \mathrm{rI2},\\
\mathrm{RNaseH} + \mathrm{rA1dI1} &\underset{k_{-,H,1}}{\overset{k_{+,H}}{\rightleftharpoons}} \mathrm{RNaseH}\cdot\mathrm{rA1dI1} \xrightarrow{k_{cat,H,1}} \mathrm{RNaseH} + \mathrm{dI1},\\
\mathrm{RNaseH} + \mathrm{A2rI2} &\underset{k_{-,H,2}}{\overset{k_{+,H}}{\rightleftharpoons}} \mathrm{RNaseH}\cdot\mathrm{A2rI2} \xrightarrow{k_{cat,H,2}} \mathrm{RNaseH} + \mathrm{A2}.
\end{aligned}
$$

Here, we do not consider side-reactions or incomplete production and degradation products. We use the superscript F to indicate template or substrate species not bound to enzymes. Thus, for instance, the total concentrations of ON-state switch is the sum of concentrations of free switch and enzyme-bound switch: $[\mathrm{T}_{ij}\mathrm{A}_j] = [\mathrm{T}_{ij}\mathrm{A}_j^F] + [\mathrm{RNAP}\cdot\mathrm{T}_{ij}\mathrm{A}_j]$. The Michaelis–Menten enzyme reactions are further simplified by the assumption that the concentrations of enzyme-substrate complexes are low compared to total substrate concentrations. Therefore, available enzyme concentrations are calculated in terms of total enzyme concentrations and substrate concentrations as follows:

$$
\begin{aligned}
[\mathrm{RNAP}^{\mathrm{tot}}] &= [\mathrm{RNAP}] + \sum_{i,j}\left([\mathrm{RNAP}\cdot\mathrm{T}_{ij}\mathrm{A}_j] + [\mathrm{RNAP}\cdot\mathrm{T}_{ij}]\right),\\
&= [\mathrm{RNAP}] + \sum_{i,j}\left(\frac{[\mathrm{RNAP}][\mathrm{T}_{ij}\mathrm{A}_j^F]}{K_{M,ON,ij}} + \frac{[\mathrm{RNAP}][\mathrm{T}_{ij}^F]}{K_{M,OFF,ij}}\right),\\
&\simeq [\mathrm{RNAP}] + \sum_{i,j}\left(\frac{[\mathrm{RNAP}][\mathrm{T}_{ij}\mathrm{A}_j]}{K_{M,ON,ij}} + \frac{[\mathrm{RNAP}][\mathrm{T}_{ij}]}{K_{M,OFF,ij}}\right),\\
[\mathrm{RNaseH}^{\mathrm{tot}}] &= [\mathrm{RNaseH}] + [\mathrm{RNaseH}\cdot\mathrm{rA1dI1}] + [\mathrm{RNaseH}\cdot\mathrm{A2rI2}],\\
&= [\mathrm{RNaseH}] + \frac{[\mathrm{RNaseH}][\mathrm{rA1dI1}^F]}{K_{M,H,1}} + \frac{[\mathrm{RNaseH}][\mathrm{A2rI2}^F]}{K_{M,H,2}},\\
&\simeq [\mathrm{RNaseH}] + \frac{[\mathrm{RNaseH}][\mathrm{rA1dI1}]}{K_{M,H,1}} + \frac{[\mathrm{RNaseH}][\mathrm{A2rI2}]}{K_{M,H,2}},
\end{aligned}
$$

where the superscript tot indicates that all complexes containing that species are considered. The Michaelis constants, the affinity of substrates to the enzymes, are calculated as $K_M = \frac{k_- + k_{cat}}{k_+}$. Thus, we express the available enzyme concentrations as follows:

$$
[\mathrm{RNAP}] = \frac{[\mathrm{RNAP}^{\mathrm{tot}}]}{1 + \sum_{i,j}\left(\frac{[\mathrm{T}_{ij}\mathrm{A}_j]}{K_{M,ON,ij}} + \frac{[\mathrm{T}_{ij}]}{K_{M,OFF,ij}}\right)}, \qquad [\mathrm{RNaseH}] = \frac{[\mathrm{RNaseH}^{\mathrm{tot}}]}{1 + \frac{[\mathrm{rA1dI1}]}{K_{M,H,1}} + \frac{[\mathrm{A2rI2}]}{K_{M,H,2}}}. \tag{1}
$$

The approximation used in equation 1 is reasonable for RNase H because a typical reaction mixture contains about 10 nM of RNase H, while its substrate concentrations are hundreds of nM. However, for RNAP, both the enzyme concentration and the switch concentrations are on the order of 100 nM such that the approximation method may not be valid. Thus, we calculate the available RNAP concentrations as follows:

$$
\begin{aligned}
[\mathrm{RNAP}\cdot\mathrm{T}_{ij}\mathrm{A}_j] &= \frac{[\mathrm{RNAP}][\mathrm{T}_{ij}\mathrm{A}_j^F]}{K_{M,ON,ij}} = \frac{[\mathrm{RNAP}]([\mathrm{T}_{ij}\mathrm{A}_j] - [\mathrm{RNAP}\cdot\mathrm{T}_{ij}\mathrm{A}_j])}{K_{M,ON,ij}},\\
[\mathrm{RNAP}\cdot\mathrm{T}_{ij}\mathrm{A}_j] &= \frac{[\mathrm{RNAP}][\mathrm{T}_{ij}\mathrm{A}_j]}{K_{M,ON,ij} + [\mathrm{RNAP}]}.
\end{aligned}
$$

Similarly,

$$[\mathrm{RNAP}\cdot \mathrm{T}_{ij}] = \frac{[\mathrm{RNAP}][\mathrm{T}_{ij}]}{K_{M,OFF,ij} + [\mathrm{RNAP}]}.$$

So that

$$\begin{aligned}
[\mathrm{RNAP}^{\mathrm{tot}}] &= [\mathrm{RNAP}] + \sum_{i,j}([\mathrm{RNAP}\cdot \mathrm{T}_{ij}\mathrm{A}_j] + [\mathrm{RNAP}\cdot \mathrm{T}_{ij}]), \qquad (2)\\
&= [\mathrm{RNAP}]\left(1 + \frac{[\mathrm{T21A1}]}{K_{M,ON,21} + [\mathrm{RNAP}]} + \frac{[\mathrm{T12A2}]}{K_{M,ON,12} + [\mathrm{RNAP}]}\right.\\
&\quad \left. + \frac{[\mathrm{T21}]}{K_{M,OFF,21} + [\mathrm{RNAP}]} + \frac{[\mathrm{T12}]}{K_{M,OFF,12} + [\mathrm{RNAP}]}\right).
\end{aligned}$$

The available RNAP concentration in equation 2 was not solved analytically but was estimated numerically by Newton's method (c.f. Martin and Coleman (1987) where RNA polymerase bound template concentration was solved analytically).

Thus, the dynamics of the Design I oscillator is described by the following seven ordinary differential equations:

$$\begin{aligned}
\frac{d[\mathrm{T21}]}{dt} &= -k_{TA,21}[\mathrm{T21}][\mathrm{A1}] + k_{TAI,21}[\mathrm{T21A1}][\mathrm{dI1}],\\
\frac{d[\mathrm{A1}]}{dt} &= -k_{AI,1}[\mathrm{A1}][\mathrm{dI1}] - k_{TA,21}[\mathrm{T21}][\mathrm{A1}] + k_{AIrA,1}[\mathrm{A1dI1}][\mathrm{rA1}],\\
\frac{d[\mathrm{dI1}]}{dt} &= -k_{AI,1}[\mathrm{A1}][\mathrm{dI1}] - k_{rAI,1}[\mathrm{rA1}][\mathrm{dI1}] - k_{TAI,21}[\mathrm{T21A1}][\mathrm{dI1}] + \frac{k_{cat,H,1}}{K_{M,H,1}}[\mathrm{RNaseH}][\mathrm{rA1dI1}],\\
\frac{d[\mathrm{rA1}]}{dt} &= -k_{rAI,1}[\mathrm{rA1}][\mathrm{dI1}] - k_{AIrA,1}[\mathrm{A1dI1}][\mathrm{rA1}] + \frac{k_{cat,ON,12}}{K_{M,ON,12} + [\mathrm{RNAP}]}[\mathrm{RNAP}][\mathrm{T12A2}]\\
&\quad + \frac{k_{cat,OFF,12}}{K_{M,OFF,12} + [\mathrm{RNAP}]}[\mathrm{RNAP}][\mathrm{T12}],\\
\frac{d[\mathrm{T12}]}{dt} &= -k_{TA,12}[\mathrm{T12}][\mathrm{A2}] + k_{TAI,12}[\mathrm{T12A2}][\mathrm{rI2}],\\
\frac{d[\mathrm{A2}]}{dt} &= -k_{AI,2}[\mathrm{A2}][\mathrm{rI2}] - k_{TA,12}[\mathrm{T12}][\mathrm{A2}] + \frac{k_{cat,H,2}}{K_{M,H,2}}[\mathrm{RNaseH}][\mathrm{A2rI2}],\\
\frac{d[\mathrm{rI2}]}{dt} &= -k_{AI,2}[\mathrm{A2}][\mathrm{rI2}] - k_{TAI,12}[\mathrm{T12A2}][\mathrm{rI2}] + \frac{k_{cat,ON,21}}{K_{M,ON,21} + [\mathrm{RNAP}]}[\mathrm{RNAP}][\mathrm{T21A1}]\\
&\quad + \frac{k_{cat,OFF,21}}{K_{M,OFF,21} + [\mathrm{RNAP}]}[\mathrm{RNAP}][\mathrm{T21}].
\end{aligned}$$

The system preserves the conservation relation, $[\mathrm{T}ij^{\mathrm{tot}}] = [\mathrm{T}ij] + [\mathrm{T}ij\mathrm{A}j]$, and similarly for $[\mathrm{A}j^{\mathrm{tot}}]$ and $[\mathrm{dI1}^{\mathrm{tot}}]$, where the superscript tot indicates that all species involving the given strands are being counted. Using these conserved quantities, the remaining variables, [T21A1], [A1dI1], [rA1dI1], [T12A2] and [A2rI2], are directly calculated from the concentrations of other species.

1.5 A detailed model of the amplified negative feedback oscillator (Design II)

Here, we introduce a new template T11 to the Design I oscillator, resulting in positive autoregulation on the amount of rA1. Four new reactions are needed, with 6 new rate constants (since for each enzyme we use only k_M and k_{cat}).

Additional hybridization and branch migration reactions

$$\begin{aligned}
\mathrm{T11} + \mathrm{A1} &\xrightarrow{k_{TA,11}} \mathrm{T11A1} && \text{(Activation)},\\
\mathrm{T11A1} + \mathrm{dI1} &\xrightarrow{k_{TAI,11}} \mathrm{T11} + \mathrm{A1dI1} && \text{(Inhibition)}.
\end{aligned}$$

Additional enzyme reactions

$$\begin{aligned}
\mathrm{RNAP} + \mathrm{T11A1} &\underset{k_{-,ON,11}}{\overset{k_+}{\rightleftharpoons}} \mathrm{RNAP}\cdot\mathrm{T11A1} \xrightarrow{k_{cat,ON,11}} \mathrm{RNAP} + \mathrm{T11A1} + \mathrm{rA1} \\
\mathrm{RNAP} + \mathrm{T11} &\underset{k_{-,OFF,11}}{\overset{k_+}{\rightleftharpoons}} \mathrm{RNAP}\cdot\mathrm{T11} \xrightarrow{k_{cat,OFF,11}} \mathrm{RNAP} + \mathrm{T11} + \mathrm{rA1}
\end{aligned}$$

The dynamics of the oscillator with this positive feedback loop can be described by eight ordinary differential equations where a differential equation for the new species [T11] is added and appropriate adjustments for the differential equations for [A1], [dI1], and [rA1] are made as follows:

$$\begin{aligned}
\frac{d[\mathrm{T11}]}{dt} &= -k_{TA,11}[\mathrm{T11}][\mathrm{A1}] + k_{TAI,11}[\mathrm{T11A1}][\mathrm{dI1}], \\
\frac{d[\mathrm{A1}]}{dt} &= -k_{AI,1}[\mathrm{A1}][\mathrm{dI1}] - k_{TA,21}[\mathrm{T21}][\mathrm{A1}] - k_{TA,11}[\mathrm{T11}][\mathrm{A1}] + k_{AIrA,1}[\mathrm{A1dI1}][\mathrm{rA1}], \\
\frac{d[\mathrm{dI1}]}{dt} &= -k_{AI,1}[\mathrm{A1}][\mathrm{dI1}] - k_{rAI,1}[\mathrm{rA1}][\mathrm{dI1}] - k_{TAI,21}[\mathrm{T21A1}][\mathrm{dI1}] - k_{TAI,11}[\mathrm{T11A1}][\mathrm{dI1}] \\
&\quad + \frac{k_{cat,H,1}}{K_{M,H,1}}[\mathrm{RNaseH}][\mathrm{rA1dI1}], \\
\frac{d[\mathrm{rA1}]}{dt} &= -k_{rAI,1}[\mathrm{rA1}][\mathrm{dI1}] - k_{AIrA,1}[\mathrm{A1dI1}][\mathrm{rA1}] + \frac{k_{cat,ON,12}}{K_{M,ON,12} + [\mathrm{RNAP}]}[\mathrm{RNAP}][\mathrm{T12A2}] \\
&\quad + \frac{k_{cat,OFF,12}}{K_{M,OFF,12} + [\mathrm{RNAP}]}[\mathrm{RNAP}][\mathrm{T12}] + \frac{k_{cat,ON,11}}{K_{M,ON,11} + [\mathrm{RNAP}]}[\mathrm{RNAP}][\mathrm{T11A1}] \\
&\quad + \frac{k_{cat,OFF,11}}{K_{M,OFF,11} + [\mathrm{RNAP}]}[\mathrm{RNAP}][\mathrm{T11}].
\end{aligned}$$

In addition, the calculation of available RNAP concentration is adjusted as follows:

$$\begin{aligned}
[\mathrm{RNAP^{tot}}] &= [\mathrm{RNAP}]\left(1 + \frac{[\mathrm{T21A1}]}{K_{M,ON,21} + [\mathrm{RNAP}]} + \frac{[\mathrm{T12A2}]}{K_{M,ON,12} + [\mathrm{RNAP}]} + \frac{[\mathrm{T11A1}]}{K_{M,ON,11} + [\mathrm{RNAP}]}\right. \\
&\quad \left. + \frac{[\mathrm{T21}]}{K_{M,OFF,21} + [\mathrm{RNAP}]} + \frac{[\mathrm{T12}]}{K_{M,OFF,12} + [\mathrm{RNAP}]} + \frac{[\mathrm{T11}]}{K_{M,OFF,11} + [\mathrm{RNAP}]}\right).
\end{aligned}$$

The Michaelis constants of switch Sw11 are expected to be similar to those of switch Sw21 due to their identical promoter structures and the catalytic constants of switch Sw11 are expected to be similar to those of switch Sw12 due to their identical output sequences. However, hybridization kinetics of switch Sw11 was not assumed to be identical to that of Sw21 because the fluorophore-quencher interaction can stabilize the T21A1 complex compared to the T11A1 complex (5). The differential equations of [T21], [T12], [A2], and [rI2] do not need adjustments after the introduction of T11. As before, [T21A1], [A1dI1], [rA1dI1], [T11A1], [T12A2], and [A2rI2] are calculated from the conservation relation.

1.6 A detailed model of the three-switch ring oscillator (Design III)

For the Design III oscillator, individual switch reactions are described by three ordinary differential equations such that the system dynamics can be described by nine differential equations. Take the switch Sw12 as an example, which was also used as a component of the Design I and Design II oscillators. The dynamics of Sw12 components are described by a similar set of ordinary differential equations as in section 1.4. In

fact, the only difference is that the RNA signal rI2 is produced by switch Sw23 rather than by switch Sw21.

$$\begin{aligned}
\frac{d[\mathrm{T12}]}{dt} &= -k_{TA,12}[\mathrm{T12}][\mathrm{A2}] + k_{TAI,12}[\mathrm{T12A2}][\mathrm{rI2}] \\
\frac{d[\mathrm{A2}]}{dt} &= -k_{AI,2}[\mathrm{A2}][\mathrm{rI2}] - k_{TA,12}[\mathrm{T12}][\mathrm{A2}] + \frac{k_{cat,H,2}}{K_{M,H,2}}[\mathrm{RNaseH}][\mathrm{A2rI2}] \\
\frac{d[\mathrm{rI2}]}{dt} &= -k_{AI,2}[\mathrm{A2}][\mathrm{rI2}] - k_{TAI,12}[\mathrm{T12A2}][\mathrm{rI2}] + \frac{k_{cat,ON,23}}{K_{M,ON,23} + [\mathrm{RNAP}]}[\mathrm{RNAP}][\mathrm{T23A3}] \\
&\quad + \frac{k_{cat,OFF,23}}{K_{M,OFF,23} + [\mathrm{RNAP}]}[\mathrm{RNAP}][\mathrm{T23}]
\end{aligned}$$

The remaining components of switch Sw12, [T12A2] and [A2rI2], are calculated from the conservation relation. The equations for the components of other switches, switch Sw31 and switch Sw23, are derived similarly.

1.7 Extended model equations including incomplete degradation products

While the detailed model was useful to develop the modeling framework and to search for desirable conditions within the parameter space, two shortcomings were apparent after experimental observation of oscillator behavior. First, the mean level of RNA concentrations kept increasing after each oscillation cycle in the gel measurements, while this phenomenon is not observed in the detailed model for a wide variety of parameter choices. Second, the experiments revealed an almost linear build-up of short degradation products, while the detailed model has no mechanism to produce short degradation products at all. To explain the experimental observation that the amount of RNA inhibitor in the Design I oscillator increased after each cycle and that the short RNA products build up over time, we developed an extended model where an incomplete degradation product is included in the reaction dynamics. These sets of extended model equations were used to generate simulation results in the main text as well as in the supplementary information. We propose that the consideration of incomplete degradation products can potentially explain both the slowdown of oscillation frequency and the accumulation of RNA signals. We define an incomplete degradation product sI2 as a 5' partial sequence of rI2 produced upon degradation by RNase H of rI2 in the A2rI2 complex. Due to the binding requirements of RNase H, five to seven bases of the 5' RNA sequence in an RNA-DNA hybrid substrate cannot be degraded (6). Thus, in our case, several bases of the toehold binding sequence within rI2 cannot be degraded and remain as part of the incomplete degradation product sI2.

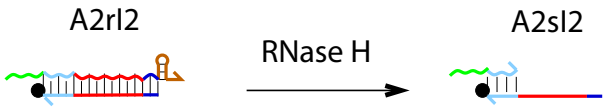

Consequently, sI2 can reversibly bind to an activator A2 or an ON-state switch T12A2, and therefore, we expect that a T12A2sI2 complex can exist. Moreover, a T12A2sI2 complex would not be efficiently inhibited by rI2 because the toehold binding sequence is not accessible.

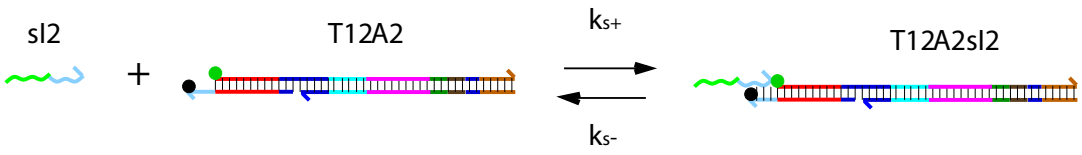

Specifically, we replaced one reaction for RNase H and added four hybridization reactions to the detailed model described earlier:

$$
\begin{aligned}
\mathrm{RNaseH} + \mathrm{A2rI2} &\underset{k_{-,H,2}}{\overset{k_{+,H}}{\rightleftharpoons}} \mathrm{RNaseH \cdot A2rI2} \xrightarrow{k_{cat,H,2}} \mathrm{RNaseH} + \mathrm{A2sI2},\\
\mathrm{A2} + \mathrm{sI2} &\underset{k_{s,-}}{\overset{k_{s,+}}{\rightleftharpoons}} \mathrm{A2sI2},\\
\mathrm{T12} + \mathrm{A2sI2} &\xrightarrow{k_{TA,12}} \mathrm{T12A2sI2},\\
\mathrm{T12A2} + \mathrm{sI2} &\underset{k_{s,-}}{\overset{k_{s,+}}{\rightleftharpoons}} \mathrm{T12A2sI2},\\
\mathrm{rI2} + \mathrm{A2sI2} &\xrightarrow{k_{AI,2}} \mathrm{A2rI2} + \mathrm{sI2},
\end{aligned}
$$

where $k_{s,+}$ is the association rate of sI2 to A2 or T12A2, $k_{s,-}$ is the dissociation rate of sI2 in A2sI2 or T12A2sI2 complex. The hybridization reaction between sI2 and A2 (or T12A2 complex) is assumed reversible because the binding site is expected to be short (˜8 bases). On the other hand, the hybridization reaction between A2sI2 and T12 (or rI2) is assumed to be identical to that of A2 and T12 (or rI2) and that rI2 can displace sI2 from A2sI2 complex because a large part of A2 sequence is available for binding within A2sI2 complex. We also assume that for the ON-state switch with the incomplete degradation product, the T12A2sI2 complex, the production rate of output rA1 is as fast as that of an unencumbered ON-state switch itself, yet inhibition by rI2 does not take place. This required expanding the equations for switch Sw12 to six dimensions as follows:

$$
\begin{aligned}
\frac{d[\mathrm{T12}]}{dt} &= -k_{TA,12}[\mathrm{T12}][\mathrm{A2}] + k_{TAI,12}[\mathrm{T12A2}][\mathrm{rI2}] - k_{TA,12}[\mathrm{T12}][\mathrm{A2sI2}],\\
\frac{d[\mathrm{A2}]}{dt} &= -k_{AI,2}[\mathrm{A2}][\mathrm{rI2}] - k_{TA,12}[\mathrm{T12}][\mathrm{A2}] - k_{s,+}[\mathrm{A2}][\mathrm{sI2}] + k_{s,-}[\mathrm{A2sI2}],\\
\frac{d[\mathrm{rI2}]}{dt} &= -k_{AI,2}[\mathrm{A2}][\mathrm{rI2}] - k_{AI,2}[\mathrm{A2sI2}][\mathrm{rI2}] - k_{TAI,12}[\mathrm{T12A2}][\mathrm{rI2}]\\
&\quad + \frac{k_{cat,ON,21}}{K_{M,ON,21} + [\mathrm{RNAP}]}[\mathrm{RNAP}][\mathrm{T21A1}] + \frac{k_{cat,OFF,21}}{K_{M,OFF,21} + [\mathrm{RNAP}]}[\mathrm{RNAP}][\mathrm{T21}],\\
\frac{d[\mathrm{sI2}]}{dt} &= -k_{s,+}[\mathrm{A2}][\mathrm{sI2}] + k_{s,-}[\mathrm{A2sI2}] + k_{AI,2}[\mathrm{A2sI2}][\mathrm{rI2}] - k_{s,+}[\mathrm{T12A2}][\mathrm{sI2}]\\
&\quad + k_{s,-}[\mathrm{T12A2sI2}],\\
\frac{d[\mathrm{A2sI2}]}{dt} &= k_{s,+}[\mathrm{A2}][\mathrm{sI2}] - k_{s,-}[\mathrm{A2sI2}] - k_{AI,2}[\mathrm{A2sI2}][\mathrm{rI2}] - k_{TA,12}[\mathrm{T12}][\mathrm{A2sI2}]\\
&\quad + \frac{k_{cat,H,2}}{K_{M,H,2}}[\mathrm{RNaseH}][\mathrm{A2rI2}],\\
\frac{d[\mathrm{T12A2sI2}]}{dt} &= k_{s,+}[\mathrm{T12A2}][\mathrm{sI2}] - k_{s,-}[\mathrm{T12A2sI2}] + k_{TA,12}[\mathrm{T12}][\mathrm{A2sI2}].
\end{aligned}
$$

The remaining variables for switch Sw12, [T12A2] and [A2rI2], are calculated from the conservation relation. Furthermore, RNA activator rA1 is transcribed from T12A2sI2 in addition to T12A2 and T12:

$$
\begin{aligned}
\frac{d[\mathrm{rA1}]}{dt} &= -k_{rAI,1}[\mathrm{rA1}][\mathrm{dI1}] - k_{AIrA,1}[\mathrm{A1dI1}][\mathrm{rA1}] + \frac{k_{cat,ON,12}}{K_{M,ON,12} + [\mathrm{RNAP}]}[\mathrm{RNAP}]\left([\mathrm{T12A2}] + [\mathrm{T12A2sI2}]\right)\\
&\quad + \frac{k_{cat,OFF,12}}{K_{M,OFF,12} + [\mathrm{RNAP}]}[\mathrm{RNAP}][\mathrm{T12}].
\end{aligned}
$$

The remaining variables for switch Sw21 do not need adjustments after the introduction of sI2. Interestingly, the toehold-binding sequence of rA1 lies close to its 3' end where degradation of RNA can be complete. It is possible that the lack of interfering signal (short rA1 that binds to the toehold sequence) may keep the excitatory connection effective with a small amount of RNA activator rA1 throughout the reaction, although further experimental verification would be required. A similar set of adjustments was implemented for the Design III oscillator model, where all three inhibitory connections mediated by rI1, rI2, and rI3, can potentially be affected by the build-up of incomplete degradation products.

1.8 Random sampling technique in the detailed model

In order to choose initial experimental parameters, such as DNA and enzyme concentrations, a natural approach would be to use the detailed model with our 'best guess' rate constants, and to use numerical gradient descent or another optimization technique to find the experimental parameters that yield the best oscillatory behavior. However, because of our uncertainties in the rate constants (prior to performing any experiments) as well as inevitable imperfections of the model, such an approach might yield experimental parameters that are far from the experimental oscillatory regime. To decrease the likelihood of this occurring, we chose a different approach for choosing initial experimental parameters: to find experimental parameters that most robustly yield oscillations under a range of rate constants.

Inspired by random sampling—high dimensional model representation (RS-HDMR) methods (1), a global analysis technique to estimate sensitivities of circuit properties with respect to circuit model parameters, we employed a random sampling technique to guide experimental parameter choices that lead to stable oscillations. We set the enzyme parameters at default values as shown below based on our previous study (2).

Parameters	
$K_{M,ON}$ (nM)	100
$k_{cat,ON}$ (/s)	0.05
$K_{M,OFF}$ (μM)	0.4
$k_{cat,OFF}$ (/s)	0.01
$K_{M,H}$ (nM)	100
$k_{cat,H}$ (/s)	0.1

Here, we assumed that all switches have identical parameters for RNAP and all RNA signals have identical parameters for RNase H. While differences in enzyme parameters are expected, because we do not have a direct control over enzyme parameters and the sequence dependence of these parameters are poorly understood, we chose not to further assess their effects on operation of our oscillator circuits. Other experimental parameters, hybridization rates and total DNA and enzyme concentrations, are analyzed for their relation to oscillator performance. Although hybridization rates are similarly not under our direct control, the toehold length dependence of strand displacement reaction rates (Inhibition and Release reactions, Figure 1) are understood well enough such that, with slight modification in sequence domain lengths, such parameters can be tuned in principle. The most experimentally tractable changes in parameters are those of DNA species concentrations, which can be continuously and exactly tuned without any sequence modifications. Each parameter was constrained within the range as shown below and sampled in a log-uniform fashion.

Parameters	Lower limit	Upper limit
k_{TA}, k_{AI}, k_{TAI}, k_{rAI}, k_{AIrA} (/M/s)	10^3	10^5
[T^{tot}] (nM)	20	200
[A^{tot}], [dI^{tot}] (nM)	50	1000
[$RNAP^{tot}$] (nM)	5	100
[$RNaseH^{tot}$] (nM)	1	20

For each random sample of parameters, an ODE simulation is run and classified as either having acceptable oscillations or not, based on the trajectory of a chosen switch in the transcriptional circuit. If the amplitude swing of the target switch is more than 5% of its total concentration and at least two peaks are detected in a finite time window (c.f. section 3), it is considered an acceptable oscillation. For the two-switch negative feedback oscillator (Design I), the time-course of ON-state switch Sw12 was analyzed between hours 7 and 16 in the simulation to exclude the initial transient phase and excessively slow oscillations. Similarly, for the three-switch ring oscillator (Design III), the time-course of ON-state

switch Sw31 was analyzed between hours 7 and 21 in the simulation. A longer time window was given for Design III oscillator because it has more components and thus presumably oscillates slower.

For the Design I oscillator, we first sampled all 15 parameters log-uniformly for 5000 iterations to estimate the overall proportion of oscillatory trajectories; 1.6% of trajectories were counted as acceptable oscillations. Then, a single parameter was fixed (at each of 15 points in a log-scale from the lower bound to the upper bound per parameter) while all the remaining 14 parameters were randomly sampled in a log-uniform fashion for 5000 iterations and the proportion of oscillatory trajectories was recorded. The simulation results for the Design I oscillator are summarized in the following figure.

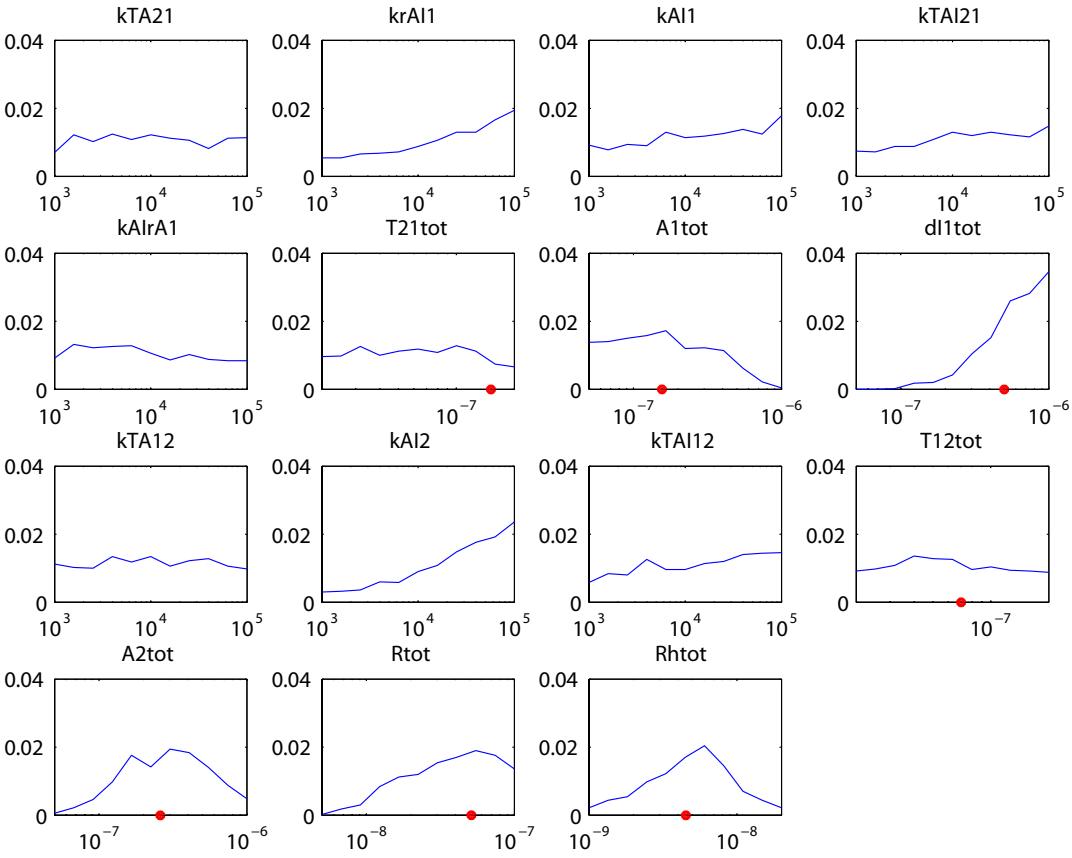

The x-axes are parameter values and y-axes are proportions of acceptable oscillations by the criteria above. Notice that the proportions of oscillations are not sensitive to certain hybridization rates, such as k_{TA}s. On the other hand, the proportion of oscillation increased with higher $k_{rAI,1}$ and $k_{AI,2}$, suggesting that fast annihilation rates help achieve oscillation, perhaps because they help establish a sharp threshold. Among the concentration parameters, the most sensitive parameter was [dI1$^{\text{tot}}$]: the oscillatory trajectory proportions increased up to 3.5% (more than twice that of the default proportion of oscillation) when it is high and no oscillation was observed when it is below 100 nM. The behavior of [A1$^{\text{tot}}$] was almost the opposite: no oscillation was detected when it is as high as 1 μM, but the oscillatory proportion increased when it is low, apparently reaching a plateau when it is between 50 and 300 nM. The concentration of the other activator strand, [A2$^{\text{tot}}$], was also a sensitive parameter: it was correlated with high proportion of oscillation when it is between 150 and 400 nM. Yet, the choice of [T$^{\text{tot}}$]s does not significantly impact oscillation. Interestingly, both [RNAP$^{\text{tot}}$] and [RNase H$^{\text{tot}}$] appear to have peaked distributions, although [RNAP$^{\text{tot}}$] has a broader peak than [RNase H$^{\text{tot}}$]. (Keep in mind, however, that the shape of all distributions depends essentially on the range of rate constants and concentrations explored in the random sampling; for example, [T21$^{\text{tot}}$] could become a sensitive parameter for some other range of parameters.)

Based on this analysis, we chose DNA and enzyme concentrations for experiment #1 (Table S5) as indicated in the plots (red dots on x-axes). This yielded damped oscillations, telling us that we were close

to the oscillatory regime and providing us with a measurable indicator of oscillator performance that could be optimized by subsequent experimental exploration.

Similarly, for the Design III oscillator, we first sampled all 17 parameters log-uniformly for 5000 iterations, finding that 0.5% of trajectories were counted as acceptable oscillations. Then, each parameter was fixed at a time while all the other parameters were sampled for 5000 iterations as above. The simulation results for the Design III oscillator are summarized in the following figure.

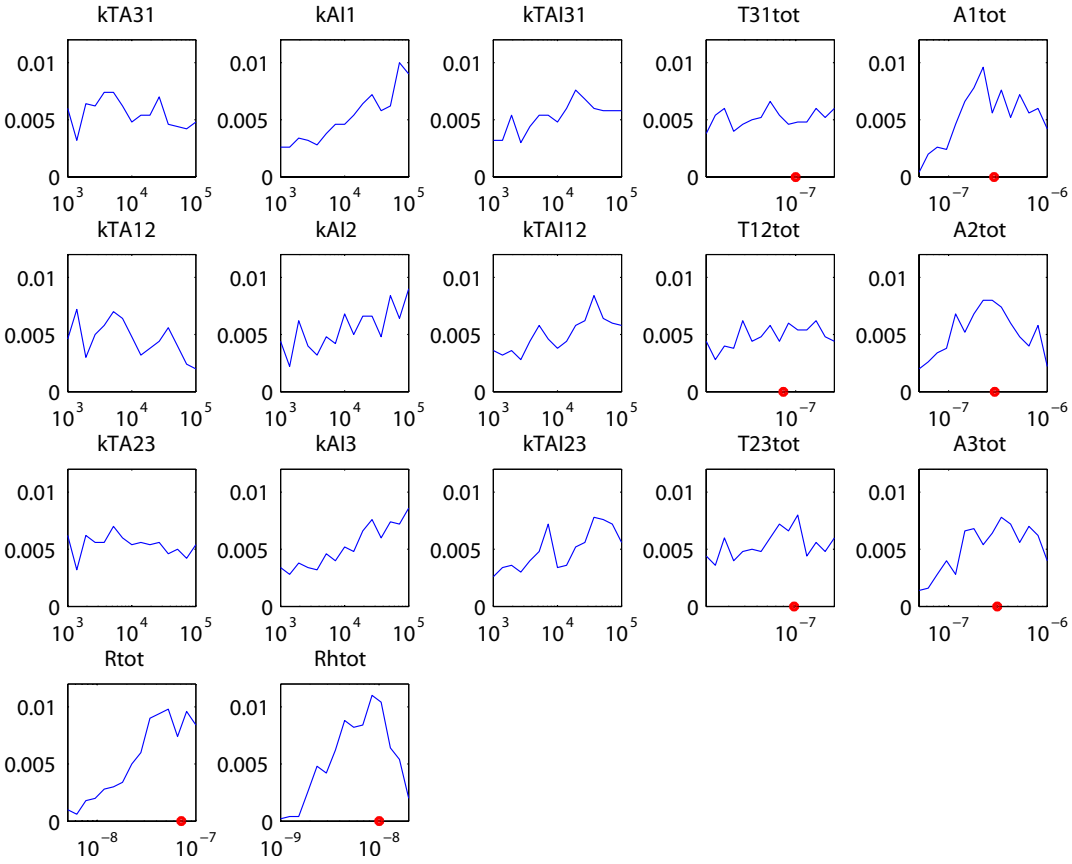

Because the three switches are all under inhibitory regulation and are assumed to have identical enzyme rate constants, the statistically averaged dependence on parameters are identical to each other. In fact, the sensitivity plots were similar to that of Sw12 in the Design I oscillator. However, the best-performing ranges of enzyme parameters were narrower compared to the Design I oscillator, possibly because properly matching switching thresholds for all three switches by random sampling was harder than for two switches, and possibly because of 'spiraling out' behavior when the RNase H is saturated (c.f. section 1.3); since 'spiraling out' behavior could cause a dramatic slowdown of oscillations over time, the above criteria could have dismissed such behavior as 'excessively slow oscillation'. In any case, based on this analysis, parameters for the initial Design III experiments (Table S7) were chosen as indicated (red dots on x-axes).

Certain aspects of the current analysis coincide with those from the simple model analysis: high thresholds for switching and high Hill exponents are both important factors to achieve stable oscillations. Also, the peaked distribution for [RNase H^{tot}] is consistent with the finding that in the simple model for Design I, γ, the ratio of time constants for degradation and hybridization, must be roughly within an order of magnitude of unity. The random sampling technique explored here provided further guidelines on the range of concentrations of individual DNA species involved and also provided insights on hybridization rates in case one would attempt to change those rates by adjusting toehold lengths.

2 Known reactions that are not modeled

The extended model does not include several reactions and species that we know to exist, because we did not think that the extra complexity was warranted. For example, RNase H will also only partially degrade rA1, yielding a short species sA1 that consists of the ~ 20 nt at the $5'$ end. However, based on fluorescence

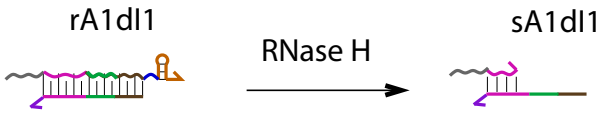

and gel results we know that Sw12 is seldom significantly ON and the levels of rA1 remain relatively low. Furthermore, although sA1 could bind to T21 and to dI1 by ~ 8 bp, at these locations it would be easily displaced by A1 or rA1. In light of these two observations, we don't expect sA1 plays a significant role in the dynamics of the Design I or Design II oscillators.

A more substantial unmodeled reaction involves rA1 binding to T21 by 18 bp to create T21rA1. This

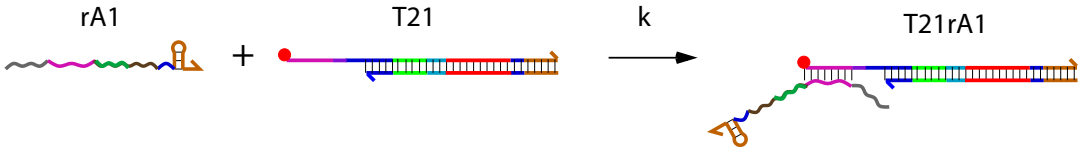

binding could in principle prevent or slow the activation of the switch by A1, however there are three ameliorating factors. First, there is a 9 base toehold in T21rA1 by which A1 can bind and displace rA1. (It was for this purpose that rA1 omitted the sequence "CTGT", resulting in four bases of dI1 ("ACAG") being unpaired in the complex rA1dI1; otherwise the toehold for A1 displacing rA1 would be a feeble 5 nt sequence "TAATA".) Second, dI1 can bind to a 16 nt region of rA1 in T21rA1 and proceed to remove rA1, which we presume to be a fast reaction. Third, the DNA:RNA hybrid in T21rA1 would serve as a substrate for RNase H, thereby degrading and removing rA1. In light of these three observations, we don't expect inclusion of these four additional reactions to significantly affect the Design I and Design II oscillator dynamics under our reaction conditions – however, we can't rule it out. (Simulation of our extended model with parameters from Table S1, augmented with these four reactions using "reasonable" parameters, were consistent with our expectations.)

3 Simulation of the extended model

The kinetic simulations and parameter fittings were implemented in MATLAB. Differential equations were solved using the *ode23s* function, while the cost function of model fits on experimental data was minimized using the *fmincon* function. An initial cost function based on least-squared errors between simulation trajectories and experimental data found local minima with non-oscillatory behavior; therefore, this cost function was abandoned. We settled on a cost function using least-squared errors of fluorescence trajectories, gel results, and characteristics of oscillation (oscillation amplitude, frequency, and damping coefficient) between simulation results and experiments. The error for each experiment is calculated as follows:

$$E = \frac{1}{\mathrm{N_f}} \sum_t ((\Delta \mathrm{TR_t})^2 + (\Delta \mathrm{TAM_t})^2) + \frac{1}{\mathrm{N_g}} \sum_t \left(\frac{\Delta \mathrm{rI}x_\mathrm{t}}{\max(\mathrm{rI}x_\mathrm{t}^\mathrm{exp}, \mathrm{rI}x_\mathrm{t}^\mathrm{sim})} \right)^2 + (\Delta \mathrm{Amp})^2 + (\Delta \mathrm{Fre})^2 + (\Delta \mathrm{Damp})^2$$

where Δ indicates the difference between experimental and simulation values, $\mathrm{N_f}$ is the number of fluorescence measurements, $\mathrm{N_g}$ is the number of gel measurements (if available), TR is the normalized Texas Red fluorescence signal (calculated as $[\mathrm{T21}]/[\mathrm{T21^{tot}}]$ for simulation results), TAM is the normalized TAMRA fluorescence signal (calculated as $[\mathrm{T12}]/[\mathrm{T12^{tot}}]$ for simulation results), $\mathrm{rI}x$ is RNA concentrations from

gel measurements, Amp is the amplitude of oscillation, Fre is the frequency of oscillation, and Damp is the damping coefficient of oscillation. For the Design I oscillator, rIx means rI2 shown in Figure 3 (reaction #37 in Figure S4 with gel results in Figure S5). For the Design II oscillator, no gel data were used. For the Design III oscillator, rIx means rI1, rI2, and rI3 shown in Figure 5 (reaction #27 in Figure S12 with gel results in Figure S11). The amplitude, frequency, and damping coefficient of each oscillation were calculated from the normalized Texas Red fluorescence signals as follows: 1. The peaks and troughs of the oscillation were marked, excluding the initial transient, by calculating derivatives of smoothed trajectories. 2. The frequency of the oscillation was calculated as follows: Fre $= 0.5*(n-1)/(t_n-t_1)$, where n is the total number of marks, t_n is the time of the last marked peak or trough, and t_1 is the time of the first marked peak or trough. 3. The amplitude is calculated as the maximum value of normalized fluorescence difference between successive marks as follows: Amp $= max_i|TR(t_i) - TR(t_{i-1})|$. 4. The damping coefficient is calculated by fitting the normalized fluorescence differences over time as an exponential decay process ($A = A_0 * e^{-\lambda t}$), where we fit $log(|TR(t_i) - TR(t_{i-1})|)$ as a linear function of time t_i to extract its slope $-\lambda$. Then, the damping coefficient is simply: Damp $= \lambda$. An example is shown below for reaction #30 of the Design I oscillator (Figure S4). The black squares correspond to peaks and troughs excluding the initial

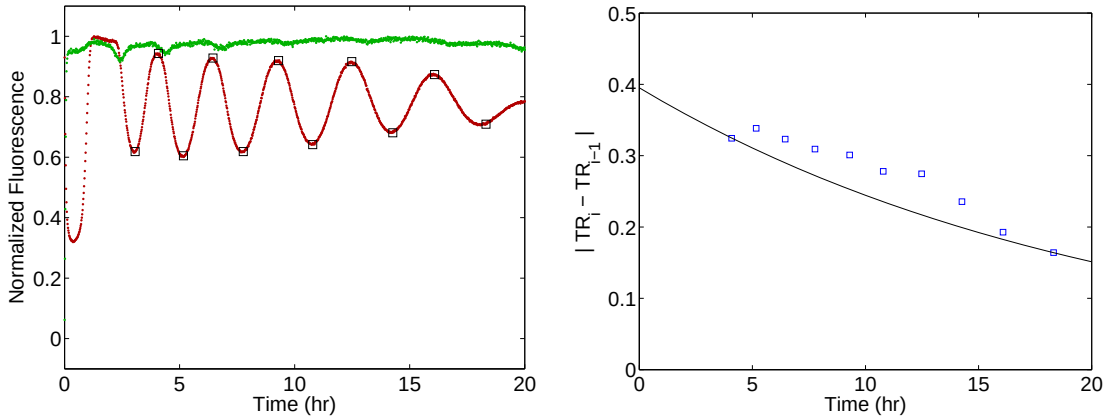

transient. In this case, five peaks and six troughs were identified, and thus, we observed five complete oscillation cycles. The difference between successive marks were plotted over time and this data was fit as an exponential decay process ($|TR(t_i) - TR(t_{i-1})| = 0.395e^{-0.048t}$). Thus, Damp = 0.048 /hr. Note that, if there were less than two marks for peaks or troughs in a given trajectory, the amplitude and frequency were assigned to be zero, and if there were less than three marks for peaks or troughs in a given trajectory, the damping coefficient defaults to 1.0. We used normalized fluorescence ranging from 0 to 1, so the maximum fluorescence error for each fluorophore will be 1. Similarly, gel error was normalized by the maximum value of experimental and simulation data at each time point. The amplitude was measured within normalized fluorescence, thus the amplitude error was less than 1. The frequency was less than 1/hr for most trajectories, and therefore frequency error was not further rescaled. The maximum damping coefficient was set to 1 when the damping coefficient was not calculated because too few peaks or troughs were detected or calculated to be more than 1. In all, the maximum error from each individual error metric was about 1. During the fit, each parameter was constrained within a plausible range spanning about two orders of magnitude as shown below.

Parameters	Lower limit	Upper limit	Other studies
$K_{M,ON}$ (nM)	10	316	15 - 37
$k_{cat,ON}$ (/s)	0.01	0.1	0.73 - 1.12
$K_{M,OFF}$ (μM)	0.1	3	0.1 - 1.1
$k_{cat,OFF}$ (/s)	0.001	0.03	0.11 - 0.18
$K_{M,H}$ (nM)	10	300	16 - 130
$k_{cat,H}$ (/s)	0.01	0.3	0.02 - 0.6
k_{TA}, k_{AI}, k_{TAI}, k_{rAI}, k_{AIrA} (/M/s)	$3*10^3$	$3*10^5$	0 - $3*10^6$
$k_{s,+}$ (/M/s)	$3*10^3$	$3*10^5$	-
$k_{s,-}$ (/s)	0.01	1	-

For comparison, the maximum hybridization rates and the range of enzyme constants from other biochemical studies are listed. (For references, see ref. (7) and references in ref. (2), Box 1.) The nominal concentrations quoted by the manufacturer were [RNAP stock] = 1.25 μM and [RNase H stock] = 1.25 μM for the enzyme stocks. Although identical in the switch components, the Design I oscillator with different enzyme batches (both RNAP and RNase H) were fit separately resulting in different parameters (Tables S1 and S2). This highlights the fact that our models have phenomenological aspects; non-modeled processes are reflected in the phenomenological rate constants. The Design II oscillator used enzyme batch #2 with a different NTP batch, thus RNAP parameters were allowed to change in addition to the new parameters for the switch Sw11 (Table S3), but other parameters were constrained to remain the same. We used a different parameter set for the Design III oscillator because several switch components are different from the Design I and Design II oscillators (Table S4). Various combinations of switch components and enzyme concentrations were explored for the three oscillator designs. Of note, the experiments were started with only RNAP for the first minute before the addition of RNase H to allow initial RNA signal build-up. Moreover, for both the Design I and Design II oscillators, the switch Sw12 was completely ON at the beginning, overproducing RNA activator rA1. Thus, except for the two reactions where manual addition of purified RNA, prior to enzyme addition, brought the initial switch states close to their steady-state values (reactions #36 and #37 in Figure S4), the first amplitude swing for the initial transient phase was much greater than the amplitudes of following oscillation cycles. In Tables S5 through S7, the concentrations of DNA and RNA species and estimated enzyme concentrations are listed.

Like many kinetic models of biological regulation, our synthetic oscillator models have poorly known parameters (8). Thus, diverse sets of reaction rate parameters are potentially compatible with experimental observation, in which similar fits can be achieved when appropriate trade-offs are made. However, our choice of parameters shows that the model we present here is quantitatively plausible compared to other biochemical studies. This is important insofar as it lends credence to the mechanistic reaction pathways used to design all three oscillators. In other studies, the T7 RNA polymerase parameters were measured on synthetic DNA templates that have a complete promoter sequence (different from our ON state template by a nick at -12) or a promoter sequence with 5 bases missing on the template side (identical to our OFF state template) (9). The higher K_M for our ON state template may be attributed to the presence of a nick. Because the transcript was very short (5 bases) in ref. (9), only the initiation rate constant was measured as k_{cat}. The initiation rate was 30 times faster than the steady-state transcription rate ("bursting") in another study (10), which may explain our small k_{cat} values. In our reaction conditions, an ON-state switch typically produced from 100 to 200 transcripts per hour when measured separately (data not shown). The RNase H parameters were measured on RNA-DNA hybrid stems of molecular beacons (11). Since our substrates (activator-inhibitor complexes) are longer than those of (11), slower k_{cat}'s are plausible. Thus, our enzyme parameters are reasonable compared to other biochemical studies. Since rA1 (or rI1 in the case of design III oscillator) is identical to the previously characterized RNA signal I1 in ref. (2), we compared the fitting parameters for enzyme reactions. The $K_{M,ON,12}$s and $k_{cat,ON,12}$s for this study ranged from 66 to 316 nM and from 0.051 to 0.081/sec, compared to a $K_{M,ON,12}$ and $k_{cat,ON,12}$ of 316 nM and 0.105/sec in (2). For an OFF-state switch, the $K_{M,OFF,12}$s and $k_{cat,OFF,12}$s of this study ranged from 1.30 to 1.61 μM and from 0.0018 to 0.017/sec, compared to 1.27 μM and 0.023/sec in our previous work. Note that the

regulatory domains are different for these switches (although they are both called Sw12 in both works) because rI2 was redesigned for this study and hence different from I2 in ref. (2). For RNase H, The $K_{M,H,1}$s and $k_{cat,H,1}$s of this study ranged from 44 to 277 nM and from 0.024 to 0.085/sec, compared to 91 nM and 0.176/sec obtained previously. Higher k_{cat}s in fitting parameters were paired with higher K_Ms. Thus, we concluded that the ON-state transcription rates and degradation rates (k_{cat}/K_M) of rA1 (rI1 in design III) are within a few fold of those in our previous study. Although maximum hybridization rates for DNA strands are reported to be on the order of 10^6/M/s (12), hybridization rate constants measured in the absence of enzymes were on the order of 10^5/M/s in our buffer conditions (data not shown), and therefore, we chose $3*10^5$/M/s as the maximum hybridization rate. In our fits, most hybridization parameters are consistently slower than 10^5/M/s, suggesting that enzyme binding or interaction with degradation products may be interfering in the hybridization reactions or strand displacement reactions. Compared to the hybridization rate parameters of (2), k_{TA}s are faster by a few fold, while k_{AI}s and k_{TAI}s are slower by a few fold.

Nevertheless, the model fits for several combinations of switch components and enzyme concentrations failed to quantitatively match experimental traces. For instance, some of the strongly damped oscillations in the experimental traces showed small but stable oscillations in simulation results (e.g., reactions #17 and #18, Figure S4). Poor fits can be expected for the initial part of fluorescence measurements due to "bursting" enzyme kinetics. At the same time, poor fits can be expected for the late part of fluorescence measurements due to buffer exhaustion, NTP depletion, and build-up of waste products. The NTP concentration was increased in an attempt to extend the lifetime of the batch reaction, and the extra Mg^{++} was added to balance the negatively charged NTPs. A complex modeling approach may improve quantitative accuracy for *in vitro* transcription systems by explicitly considering NTP, enzyme life-time, and product inhibition (13).

4 Model source files

All model source files and the experimental data used in this work are available as Supplementary Information. Author instructions are included for using MATLAB files to reproduce figures in the main text and Supplementary Information. The simple models, detailed models, and extended models (Sections 1.1–1.7) have also been converted to SBML format. Of note, the SBML files use a full Michaelis-Menten enzyme reactions rather than Michaelis-Menten approximations described in Sections 1.4–1.7. SBML files have been submitted to the BioModels database (http://www.ebi.ac.uk/biomodels/) with the accession numbers MODEL1012090000 through MODEL1012090006.

5 DNA sequences

T21-nt (101mer), 5'-\ Texas Red \-CATTAGTGTCGTTCGTTCACAGTAATACGACTCACTATAGGGAGAGTAAAACGGATTGAAGCAAGGGTAAGATGGAATGATAATACTGACAAAGTCAGAAA-3'.

T21-t (74mer), 5'-TTTCTGACTTTGTCAGTATTATCATTCCATCTTACCCTTGCTTCAATCCGTTTTACTCTCCCTATAGTGAGTCG-3'.

A1 (36mer), 5'-TATTACTGTGAACGAACGACACTAATGAACTACTAC-\ IowaBlack RQ \-3'.

dI1 (38mer), 5'-GTGTGTAGTAGTAGTTCATTAGTGTCGTTCGTTCACAG-3'.

T12-nt (106mer), 5'-\ TAMRA \-AAGCAAGGGTAAGATGGAATGATAATACGACTCACTATAGGGAGAAACAAAGAACGAACGACACTAATGAACTACTACTACACACTAATACTGACAAAGTCAGAAA-3'.

T12-t (79mer), 5'-TTTCTGACTTTGTCAGTATTAGTGTGTAGTAGTAGTTCATTAGTGTCGTTCGTTCTTTGTTTCTCCCTATAGTGAGTCG-3'.

A2 (35mer), 5'-TATTATCATTCCATCTTACCCTTGCTTCAATCCGT-\ IowaBlack RQ \-3'.

T31-nt (103mer), 5'-CTAATGAACTACTACTACACACTAATACGACTCACTATAGGGAGATCAAATTTACAACGCAACTAACATATAATCGAAGACTTAATACTGACAAAGTCAGAAA-3'.

T31-t (76mer), 5'-TTTCTGACTTTGTCAGTATTAAGTCTTCGATTATATGTTAGTTGCGTTGTAAATTTGATCTCCCTATAGTGAGTCG-3'.

A3 (35mer), 5'-TATTAAGTCTTCGATTATATGTTAGTTGCGTTGTA-3'.

A'1 (35mer), 5'-TATTAGTGTGTAGTAGTAGTTCATTAGTGTCGTTC-3'.

T23-nt (101mer), 5'-AACTAACATATAATCGAAGACTTAATACGACTCACTATAGGGAGAGTAAAACGGATTGAAGCAAGGGTAAGATGGAATGATAATACTGACAAAGTCAGAAA-3'.

References

[1] Xiao-jiang Feng, Sara Hooshangi, David Chen, Genyuan Li, Ron Weiss, and Herschel Rabitz. Optimizing genetic circuits by global sensitivity analysis. *Biophys. J.*, 87:2195–2202, 2004.

[2] Jongmin Kim, Kristin S White, and Erik Winfree. Construction of an *in vitro* bistable circuit from synthetic transcriptional switches. *Mol. Syst. Biol.*, 2:68, 2006.

[3] Joseph R. Pomerening, Eduardo D. Sontag, and James E Ferrell, Jr. Building a cell cycle oscillator: hysterisis and bistability in the activation of Cdc2. *Nature Cell Biology*, 5:346–351, 2003.

[4] Jeff Hasty, Farren Isaacs, Milos Dolnik, David McMillen, and James J. Collins. Designer gene networks: towards fundamental cellular control. *Chaos*, 11:207–220, 2001.

[5] Salvatore A. E. Marras, Fred Russell Kramer, and Sanjay Tyagi. Efficiencies of fluorescence resonance energy transfer and contact-mediated quenching in oligonucleotide probes. *Nucleic Acids Res.*, 30(21):e122, 2002.

[6] Walt F. Lima and Stanley T. Crooke. Cleavage of single strand RNA adjacent to RNA-DNA duplex regions by *Escherichia coli* RNase H1. *J. Biol. Chem.*, 272:27,513–27,516, 1997.

[7] James G. Wetmur. DNA probes: Applications of the principles of nucleic acid hybridization. *Crit. Rev. Biochem. Mol. Biol.*, 36:227–259, 1991.

[8] Kevin S Brown and James P Sethna. Statistical mechanical approaches to models with many poorly known parameters. *Phys. Rev. E*, 68:021904, 2003.

[9] Craig T. Martin and Joseph E. Coleman. Kinetic analysis of T7 RNA polymerase-promoter interactions with small synthetic promoters. *Biochemistry*, 26:2690–2696, 1987.

[10] Yiping Jia and Smita S. Patel. Kinetic mechanism of transcription initiaion by bacteriophage T7 RNA polymerase. *Biochemistry*, 36:4223–4232, 1997.

[11] J Rizzo, L K Gifford, X Zhang, A M Gewirtz, and P Lu. Chimeric RNA-DNA molecular beacon assay for ribonuclease H activity. *Mol. Cell. Probes*, 16:277–283, 2002.

[12] Bernard Yurke and Allen P. Mills, Jr. Using DNA to power nanostructures. *Genet. Program. Evol. Mach.*, 4:111–122, 2003.

[13] Sabine Arnold, Martin Siemann, Kai Scharnweber, Markus Werner, Sandra Baumann, and Matthias Reuss. Kinetic modeling and simulation of in vitro transcription by phage T7 RNA polymerase. *Biotechnol. Bioeng.*, 72:548–561, 2001.

Table S1. Model parameters for the Design I oscillator with enzyme batch #1.

	i=2, j=1	i=1, j=2	Other studies
$K_{M,ON,ij}$ (nM)	209	88	15-37
$k_{cat,ON,ij}$ (/s)	0.038	0.066	0.73-1.12
$K_{M,OFF,ij}$ (μM)	0.88	1.37	0.1-1.1
$k_{cat,OFF,ij}$ (/s)	0.0022	0.0034	0.11-0.18
$K_{M,H,j}$ (nM)	154	82	16-130
$k_{cat,H,j}$ (/s)	0.057	0.206	0.02-0.6
$k_{TA,ij}$ (/M/s)	$2.93*10^4$	$6.24*10^3$	-
$k_{AI,j}$ (/M/s)	$1.26*10^4$	$5.28*10^3$	-
$k_{TAI,ij}$ (/M/s)	$1.90*10^4$	$7.24*10^4$	-
$k_{rAI,j}$ (/M/s)	$1.34*10^4$	-	-
$k_{AIrA,j}$ (/M/s)	$1.45*10^4$	-	-
$k_{s,+}$ (/M/s)	$5.30*10^4$	-	-
$k_{s,-}$ (/s)	0.118	-	-

Table S2. Model parameters for the Design I oscillator with enzyme batch #2.

	i=2, j=1	i=1, j=2	Other studies
$K_{M,ON,ij}$ (nM)	118	113	15-37
$k_{cat,ON,ij}$ (/s)	0.026	0.081	0.73-1.12
$K_{M,OFF,ij}$ (μM)	0.48	1.61	0.1-1.1
$k_{cat,OFF,ij}$ (/s)	0.0024	0.0018	0.11-0.18
$K_{M,H,j}$ (nM)	44	55	16-130
$k_{cat,H,j}$ (/s)	0.024	0.062	0.02-0.6
$k_{TA,ij}$ (/M/s)	$6.04*10^4$	$4.63*10^3$	-
$k_{AI,j}$ (/M/s)	$1.00*10^4$	$4.28*10^4$	-
$k_{TAI,ij}$ (/M/s)	$1.03*10^4$	$2.23*10^4$	-
$k_{rAI,j}$ (/M/s)	$4.27*10^4$	-	-
$k_{AIrA,j}$ (/M/s)	$7.96*10^4$	-	-
$k_{s,+}$ (/M/s)	$1.92*10^5$	-	-
$k_{s,-}$ (/s)	0.032	-	-

Table S3. Model parameters for the Design II oscillator with enzyme batch #2.

	i=2, j=1	i=1, j=2	i=1, j=1	Other studies
$K_{M,ON,ij}$ (nM)	40	66	102	15-37
$k_{cat,ON,ij}$ (/s)	0.024	0.051	0.020	0.73-1.12
$K_{M,OFF,ij}$ (μM)	1.34	1.38	2.71	0.1-1.1
$k_{cat,OFF,ij}$ (/s)	0.0071	0.0027	0.0027	0.11-0.18
$K_{M,H,j}$ (nM)	44	55	-	16-130
$k_{cat,H,j}$ (/s)	0.024	0.062	-	0.02-0.6
$k_{TA,ij}$ (/M/s)	$6.04*10^4$	$4.63*10^3$	$5.00*10^4$	-
$k_{AI,j}$ (/M/s)	$1.00*10^4$	$4.28*10^4$	-	-
$k_{TAI,ij}$ (/M/s)	$1.03*10^4$	$2.23*10^4$	$9.61*10^3$	-
$k_{rAI,j}$ (/M/s)	$4.27*10^4$	-	-	-
$k_{AIrA,j}$ (/M/s)	$7.96*10^4$	-	-	-
$k_{s,+}$ (/M/s)	$1.92*10^5$	-	-	-
$k_{s,-}$ (/s)	0.032	-	-	-

Table S4. Model parameters for the Design III oscillator with enzyme batch #2.

	i=3, j=1	i=1, j=2	i=2, j=3	Other studies
$K_{M,ON,ij}$ (nM)	135	316	307	15-37
$k_{cat,ON,ij}$ (/s)	0.078	0.061	0.078	0.73-1.12
$K_{M,OFF,ij}$ (μM)	1.67	1.30	1.09	0.1-1.1
$k_{cat,OFF,ij}$ (/s)	0.028	0.017	0.027	0.11-0.18
$K_{M,H,j}$ (nM)	277	108	92	16-130
$k_{cat,H,j}$ (/s)	0.085	0.211	0.285	0.02-0.6
$k_{TA,ij}$ (/M/s)	$3.41*10^3$	$3.94*10^3$	$3.33*10^3$	-
$k_{AI,j}$ (/M/s)	$1.04*10^4$	$4.24*10^4$	$6.43*10^3$	-
$k_{TAI,ij}$ (/M/s)	$4.29*10^3$	$8.41*10^3$	$6.35*10^3$	-
$k_{s,+}$ (/M/s)	$4.12*10^3$	$1.31*10^4$	$6.73*10^3$	-
$k_{s,-}$ (/s)	0.83	0.62	0.59	-

Table S5. Reaction conditions for the Design I oscillator.

Reaction #	T21 (nM)	A1 (nM)	dI1 (nM)	T12 (nM)	A2 (nM)	rA1 (nM)	rI2 (nM)	RNAP (nM)	RNase H (nM)	enzyme batch #
1	150	150	500	70	250	0	0	50	4.2	1
2	150	150	500	70	250	0	0	71	6.3	1
3	200	200	500	100	250	0	0	50	4.2	1
4	200	200	500	100	250	0	0	71	6.3	1
5	250	250	500	120	250	0	0	71	6.3	1
6	250	250	500	120	250	0	0	92	8.3	1
7	250	250	700	120	350	0	0	71	6.3	1
8	250	250	700	120	350	0	0	92	8.3	1
9	250	250	700	120	350	0	0	92	10.4	1
10	250	250	700	120	450	0	0	92	10.4	1
11	250	250	700	120	350	0	0	133	15.6	1
12	250	250	700	120	450	0	0	133	15.6	1
13	250	250	1000	80	500	0	0	125	15.0	1
14	250	250	1500	80	750	0	0	125	15.0	1
15	250	250	1000	100	500	0	0	125	15.0	1
16	250	250	1500	100	750	0	0	125	15.0	1
17	250	250	1000	120	350	0	0	125	15.0	1
18	250	250	1300	120	350	0	0	125	15.0	1
19	250	250	1000	180	350	0	0	125	15.0	1
20	250	250	1200	180	450	0	0	125	15.0	1
21	150	150	1000	180	350	0	0	125	15.0	1
22	150	150	1000	180	350	0	0	125	26.0	1
23	200	200	1000	180	350	0	0	125	15.0	1
24	200	200	1000	180	350	0	0	125	26.0	1
25	250	250	700	120	350	0	0	83	9.2	2
26	250	250	700	120	350	0	0	83	11.5	2
27	250	250	1000	120	500	0	0	83	9.2	2
28	250	250	1000	120	500	0	0	83	11.5	2
29	250	250	700	120	350	0	0	125	15	2
30	250	250	700	120	350	0	0	125	17.5	2
31	250	250	1000	120	500	0	0	125	15	2
32	250	250	1000	120	500	0	0	125	17.5	2
33	250	250	700	120	350	740	0	125	17.5	2
34	250	250	700	120	350	0	370	125	17.5	2
35	250	250	700	120	350	740	370	125	17.5	2
36	250	250	700	120	350	500	370	125	17.5	2
37	250	250	1000	120	500	800	550	125	17.5	2

Table S6. Reaction conditions for the Design II oscillator with enzyme batch #2. The initial concentrations of RNA inputs were zero for this set of reactions ([rA1] = [rI2] = 0 nM).

Reaction #	T21 (nM)	A1 (nM)	dI1 (nM)	T12 (nM)	A2 (nM)	T11 (nM)	RNAP (nM)	RNase H (nM)
1	250	250	1000	100	500	0	125	17.5
2	250	250	1000	80	500	20	125	17.5
3	250	250	1000	80	500	40	125	17.5
4	250	250	1000	100	500	20	125	17.5
5	250	250	1000	60	500	0	123	13
6	250	250	1000	60	500	30	123	13
7	250	250	1000	60	500	60	123	13
8	250	250	1000	60	500	90	123	13

Table S7. Reaction conditions for the Design III oscillator with enzyme batch #2. The initial concentrations of one RNA input was zero for this set of reactions ([rI3] = 0 nM), while the others ([rI1] and [rI2]) varied.

Reaction #	T31 (nM)	A1 (nM)	T12 (nM)	A2 (nM)	T23 (nM)	A3 (nM)	rI1 (nM)	rI2 (nM)	RNAP (nM)	RNase H (nM)
1	100	300	80	300	100	300	0	600	83	10.4
2	100	400	80	300	100	300	0	600	83	10.4
3	100	300	100	300	100	300	0	600	83	10.4
4	100	400	100	300	100	300	0	600	83	10.4
5	100	250	100	250	100	250	0	500	63	9.4
6	100	250	100	250	100	250	500	0	63	9.4
7	100	300	80	300	100	300	0	600	83	10.4
8	100	300	80	400	100	300	0	600	83	10.4
9	80	300	100	300	100	300	0	600	83	10.4
10	80	300	100	300	100	400	0	600	83	10.4
11	80	300	100	250	100	400	0	600	83	10.4
12	80	300	100	300	100	400	0	600	83	10.4
13	80	300	100	250	120	400	0	600	83	10.4
14	80	300	100	300	120	400	0	600	83	10.4
15	80	250	100	250	120	400	0	500	83	10.4
16	80	400	100	250	120	400	0	500	83	10.4
17	80	300	100	200	120	400	0	500	83	10.4
18	80	300	100	250	120	500	0	500	83	10.4
19	100	300	100	160	120	400	0	400	83	10.4
20	100	300	100	160	120	400	0	400	83	12.5
21	100	300	100	200	120	400	0	400	83	10.4
22	100	300	100	200	120	400	0	400	83	12.5
23	100	300	100	200	120	400	0	0	83	10.4
24	100	300	100	200	120	400	0	200	83	10.4
25	100	300	100	200	120	400	0	0	83	10.4
26	100	300	100	200	120	400	0	0	94	11.5
27	100	300	100	200	120	400	0	0	83	10.4

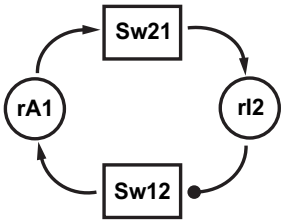

T21 A1

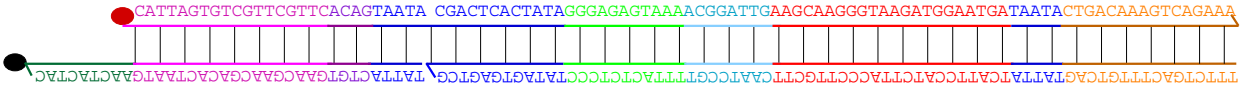

T21

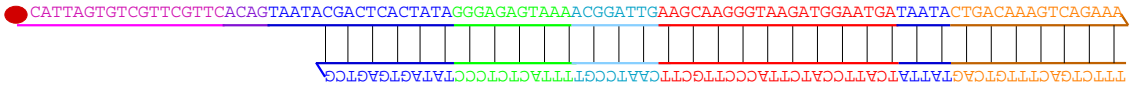

A1

dI1

A1dI1

rA1

rA1dI1

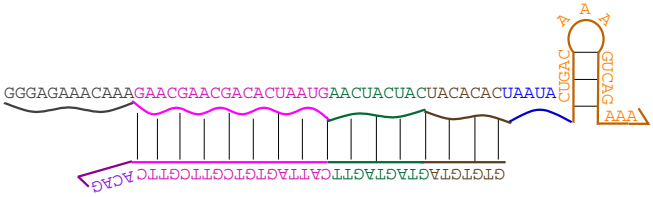

T12A2

T12

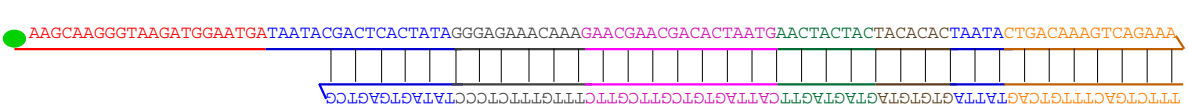

A2

rI2

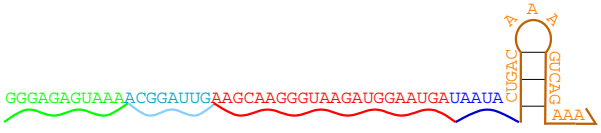

A2rI2

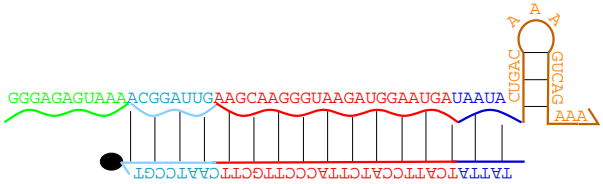

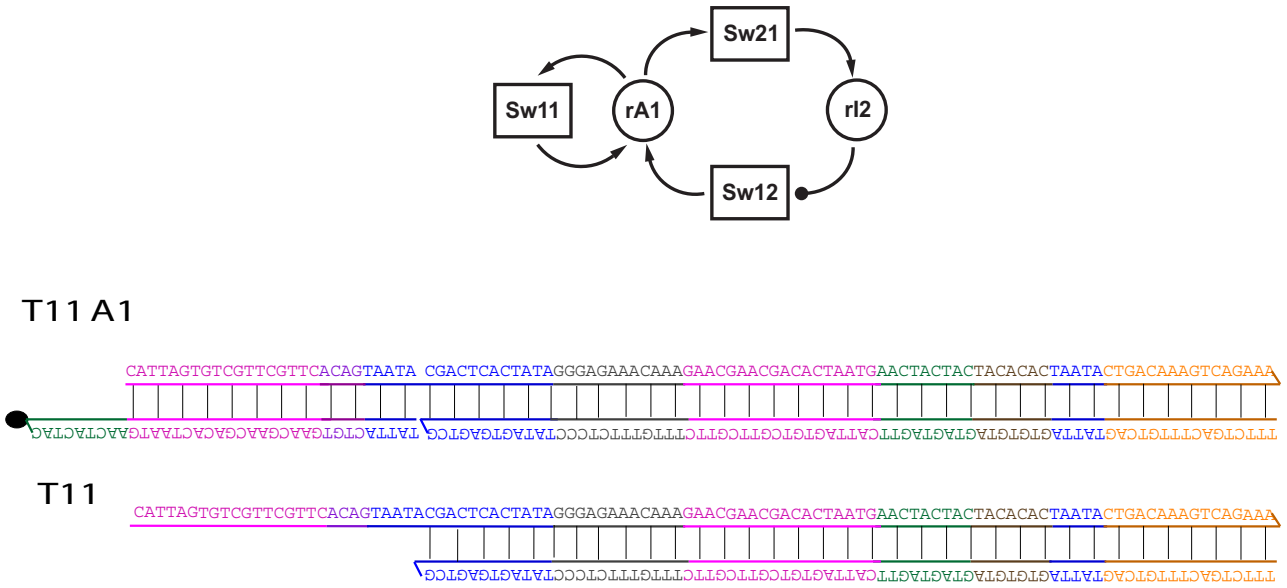

Figure S1: DNA and RNA sequences of single-stranded species and complexes for synthetic oscillators. The sequence domains are color-coded to indicate identical or complementary sequences; dark blue indicates the T7 RNAP promoter. For the Design I oscillator, the color-coding scheme is as shown in Figure 1. For the Design II oscillator, the new ON-state switch T11A1 and OFF-state switch T11 are shown. For the Design III oscillator, several DNA and RNA species are in common with those of the Design I oscillator. First, switch Sw12 is shared in both designs, and hence is not redrawn in the sequence diagram. However, the RNA activator rA1 in the Design I oscillator is used as an RNA inhibitor rI1 in the Design III oscillator. Therefore, we use a new activator A'1 that binds to rI1; compared to dI1 of Design I, the A'1 is longer by 5 more bases of missing promoter region on the 5' end and shorter by 8 bases on the 3' end. Also, T23-t is the same as T21-t coding for the same RNA inhibitor rI2. A separately designed RNA inhibitor rI3 completes the cycle.

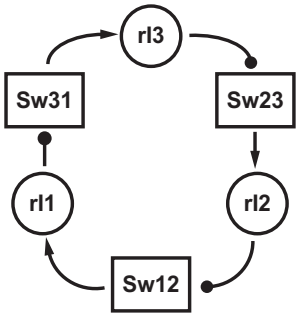

T31 A′1

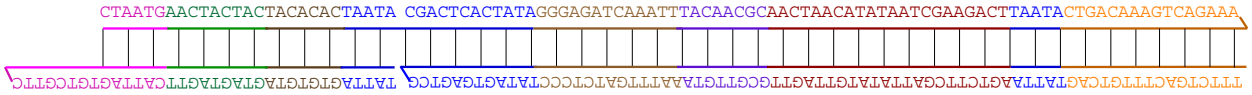

T31

A′1

rl1

A′1rl1

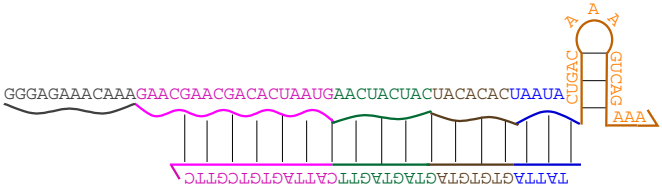

T23 A3

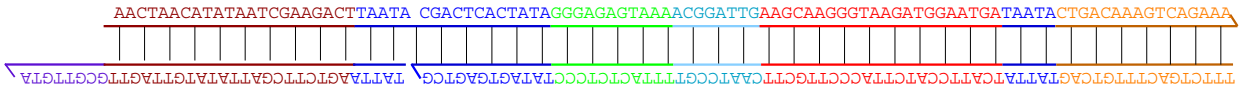

T23

A3

rl3

A3rl3

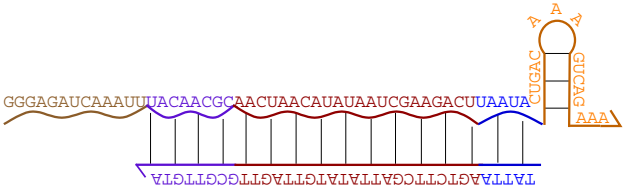

A

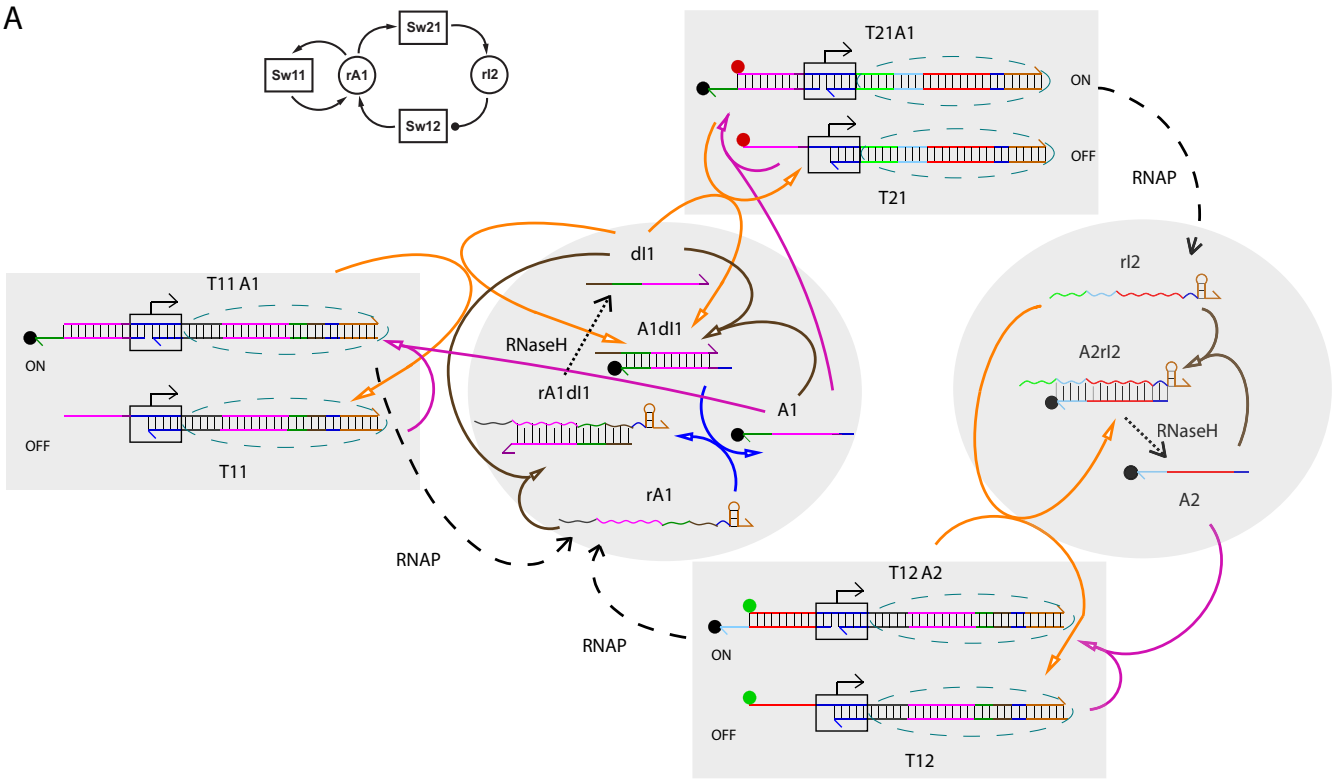

B

Activation		T11 + A1 ⟶ T11A1		T21 + A1 ⟶ T21A1		T12 + A2 ⟶ T12A2	
Inhibition		T11A1 + dI1 ⟶ T11 + A1dI1		T21A1 + dI1 ⟶ T21 + A1dI1		T12A2 + rI2 ⟶ T12 + A2rI2	
Annihilation		A1 + dI1 ⟶ A1dI1				A2 + rI2 ⟶ A2rI2	
		rA1 + dI1 ⟶ rA1dI1					
Release		A1dI1 + rA1 ⟶ rA1dI1 + A1					
RNAP	(fast)	T11A1 ⟶ T11A1 + rA1	(fast)	T21A1 ⟶ T21A1 + rI2	(fast)	T12A2 ⟶ T12A2 + rA1	
	(slow)	T11 ⟶ T11 + rA1	(slow)	T21 ⟶ T21 + rI2	(slow)	T12 ⟶ T12 + rA1	
RNaseH		rA1dI1 ⟶ dI1				A2rI2 ⟶ A2	

Figure S2: Enzyme and hybridization reactions for the amplified negative feedback oscillator (Design II, detailed model). **(A)** Reaction diagram. On the top left is a block diagram for the Design II oscillator. The detailed diagrams are color-coded as described in Fig. 1. Note that the new switch, Sw11, was not fluorophore-labeled and hence was not monitored by fluorescence. DNA and RNA sequences of single-stranded species and complexes are shown in Fig. S1. **(B)** List of hybridization and enzyme reactions. See SI text 1.5 for details.

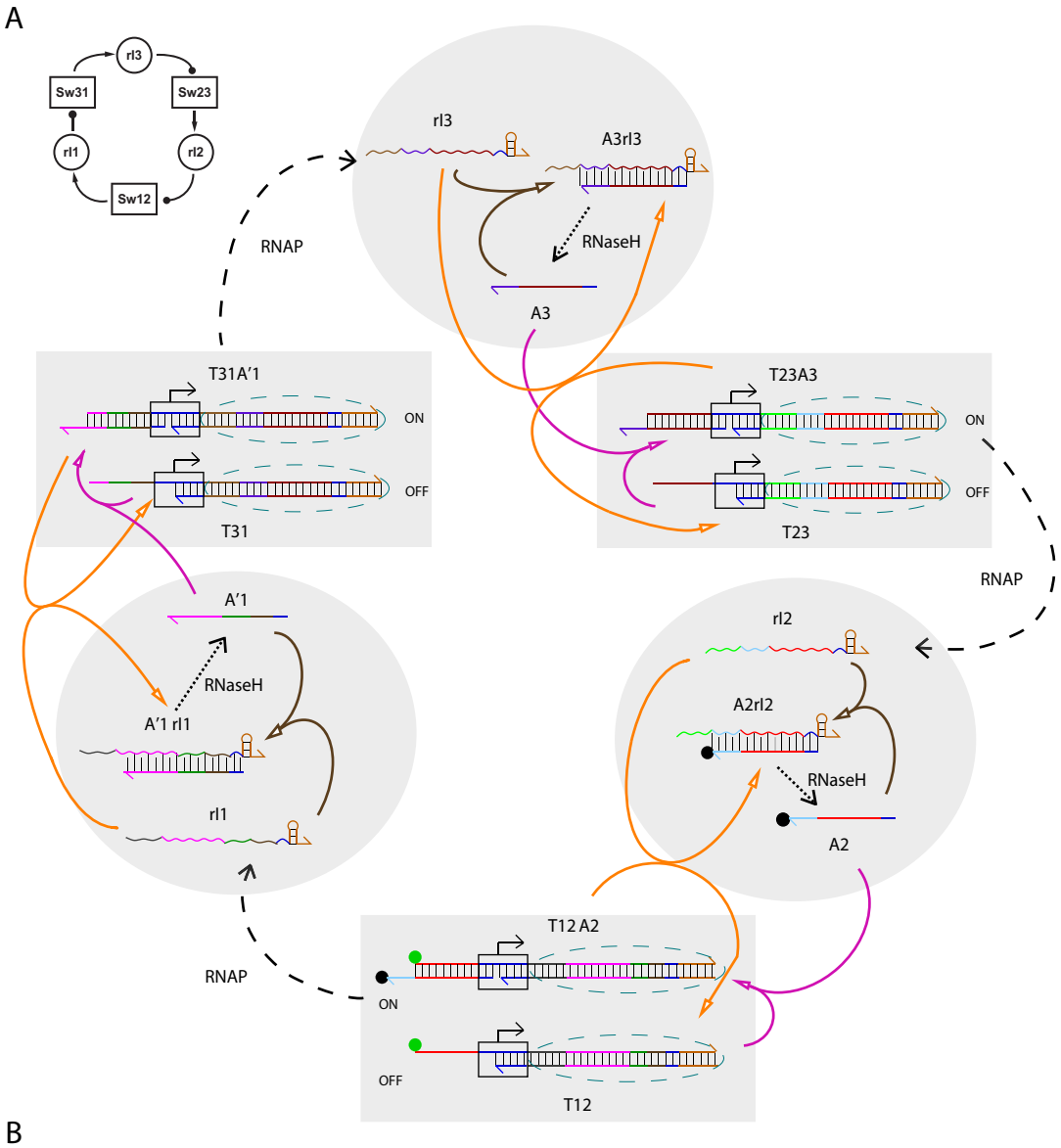

Figure S3: Enzyme and hybridization reactions for the three-switch ring oscillator (Design III, detailed model). **(A)** Reaction diagram. On the top left is a block diagram for the Design III oscillator. The detailed diagrams are color-coded as described in Fig. 1. Note that only switch Sw12 was monitored by fluorescence: OFF-state switch T12 was labeled with TAMRA (green circle), and activator A2 was labeled with Iowa Black RQ quencher (black circle). DNA and RNA sequences of single-stranded species and complexes are shown in Fig. S1. **(B)** List of hybridization and enzyme reactions. See SI text 1.6 for details.

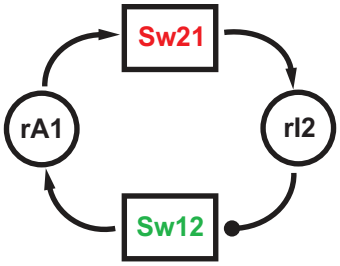
Sw21
rA1
rl2
Sw12

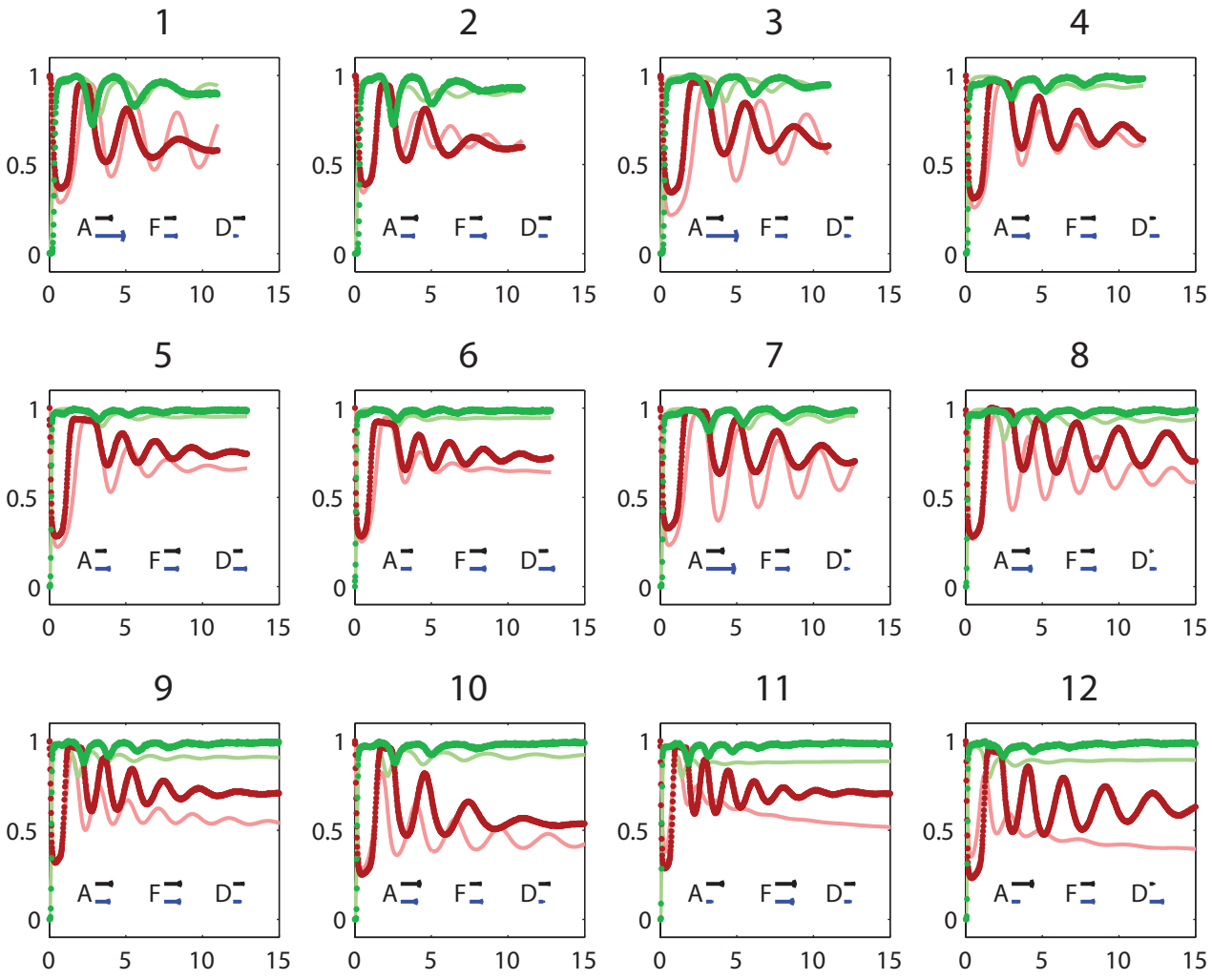
1
2
3
4
5
6
7
8
9
10
11
12
A
F
D
0
0.5
1
0
5
10
15

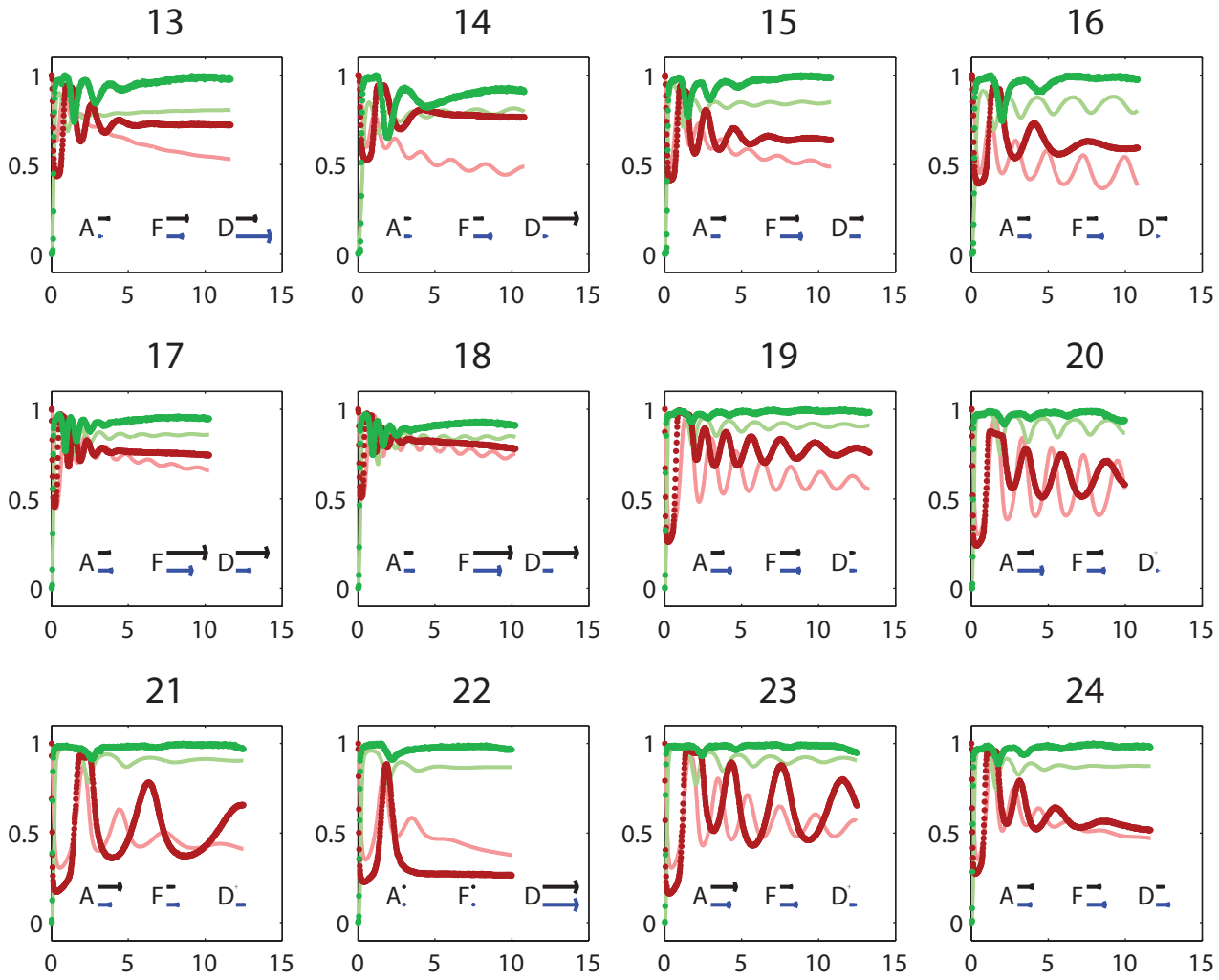

Figure S4: Experimental results and extended model fits for the two-switch negative feedback oscillator (Design I). Horizontal axes are time in hours, and vertical axes are normalized fluorescence signal. The experimental time-courses are plotted as dots and simulation time-courses are plotted as lines in lighter shades: Texas Red of T21 (red) and TAMRA of T12 (green). I.e a high fluorescence value indicates that the switch is OFF, while a low fluorescence value indicates that the switch is ON. To generate simulation time-courses, we used the parameter set listed in Table S1 for reactions #1 through #24 (enzyme batch #1). These parameters were fit using the fluorescence time-courses (reactions #1 through #24) of Design I oscillator. For reactions #25 through #37 which used enzyme batch #2, the parameter set listed in Table S2 was used. These parameters were fit using the fluorescence time-courses (reactions #25 through #37) and gel data of Design I oscillator. The amplitude (A), frequency (F), and damping coefficients (D) of oscillation for experimental and simulation trajectories are shown as black arrows and blue arrows, respectively. The experimental conditions are listed in Table S5 with the corresponding reaction numbers indicated on top of plots. Reactions #8 and #13 are shown in Figure 2 and reaction #37 is shown in Figure 3.

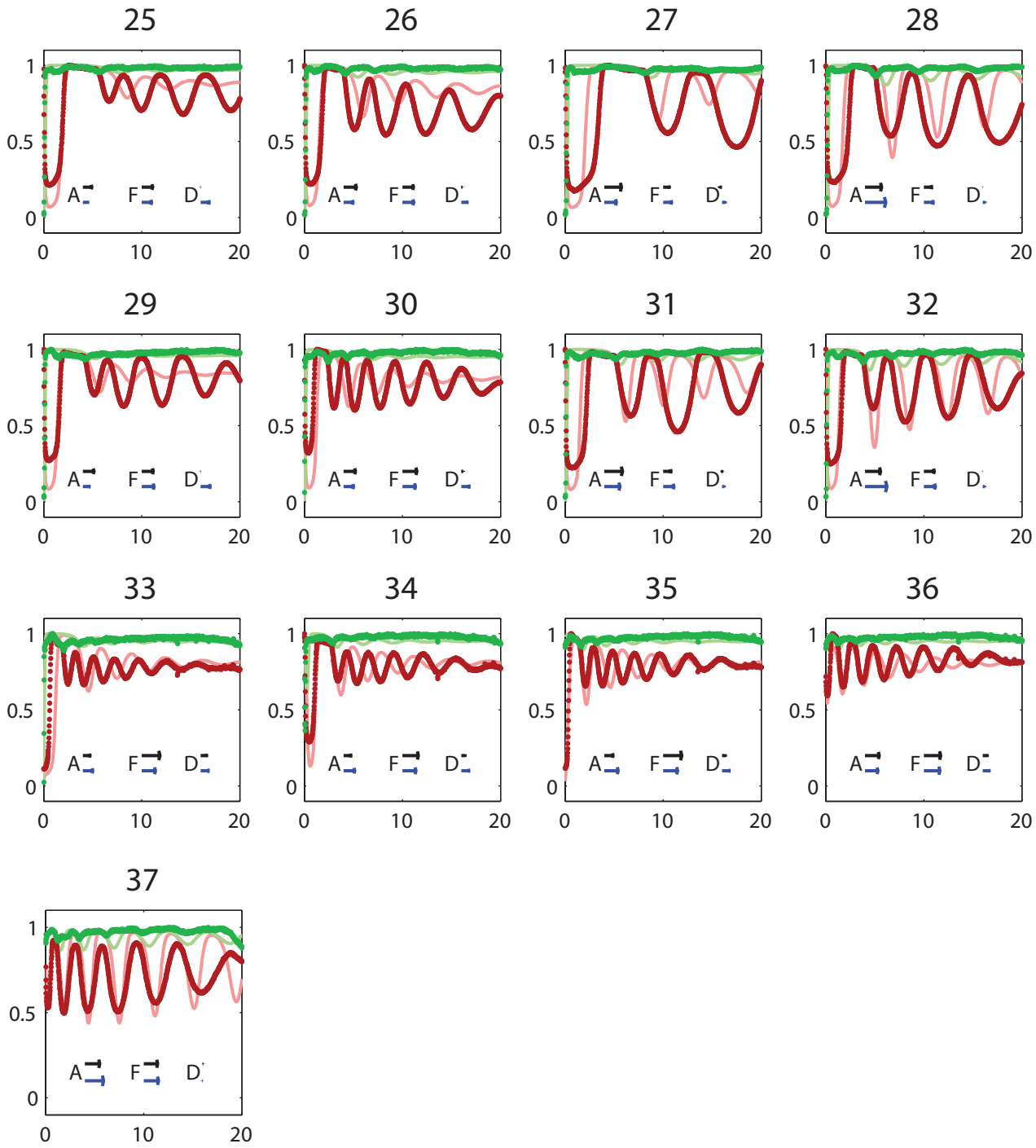
25
26
27
28
29
30
31
32
33
34
35
36
37
A
F
D
0
0.5
1
0
10
20

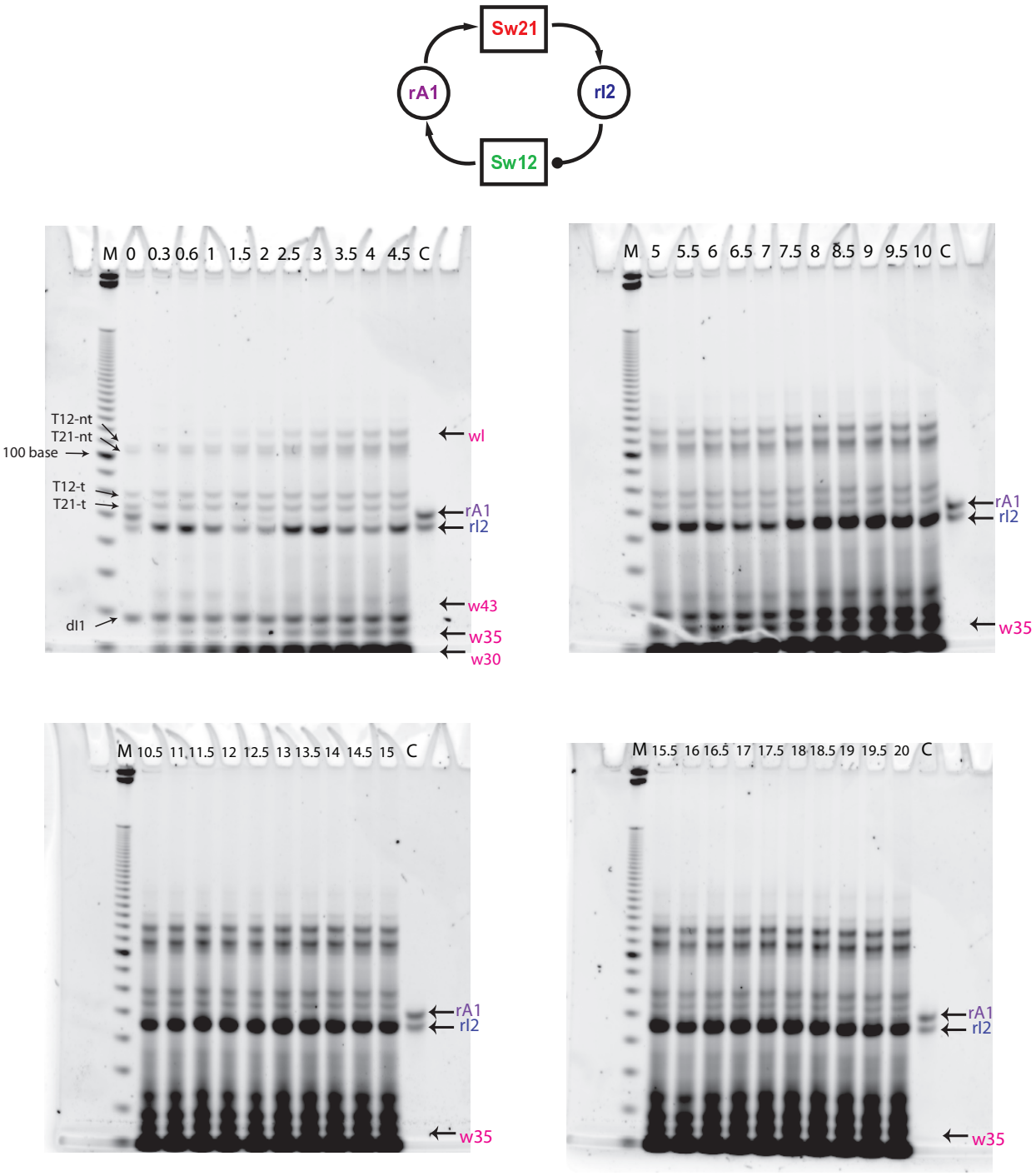

Figure S5: Denaturing gel results for the Design I oscillator. The gels are stained with SYBR gold for quantitation. Numbers above each lane mark the transcription reaction times in hours as shown in the fluorescence measurements of Figure 3A. The rI2 concentrations were measured using the rectangular box tool with respect to 1 μM of purified rI2 (62 bases) band densities in control lanes. The rA1 (67 bases) signal was not significantly above background in many cases and hence was not quantified. Several species of unknown sequences were also observed in the gel: potential self-coded elongation product of RNA transcript, wl ($>$ 100 bases), and presumed incomplete degradation products, w43 (about 43 bases), w35 (about 35 bases), and w30 ($<$ 30 bases). The concentration of incomplete degradation products shown in Figure 3B is estimated from the band of $\approx$35 nucleotides (w35, magenta). The DNA strands are also identified: T12-nt (106 bases), T21-nt (101 bases), T12-t (79 bases), T21-t (74 bases), and dI1 (38 bases). The DNA activators A1 and A2 are not clearly identified because they are labeled with quenchers. M: 10 base-pair ladder, C: control lane.

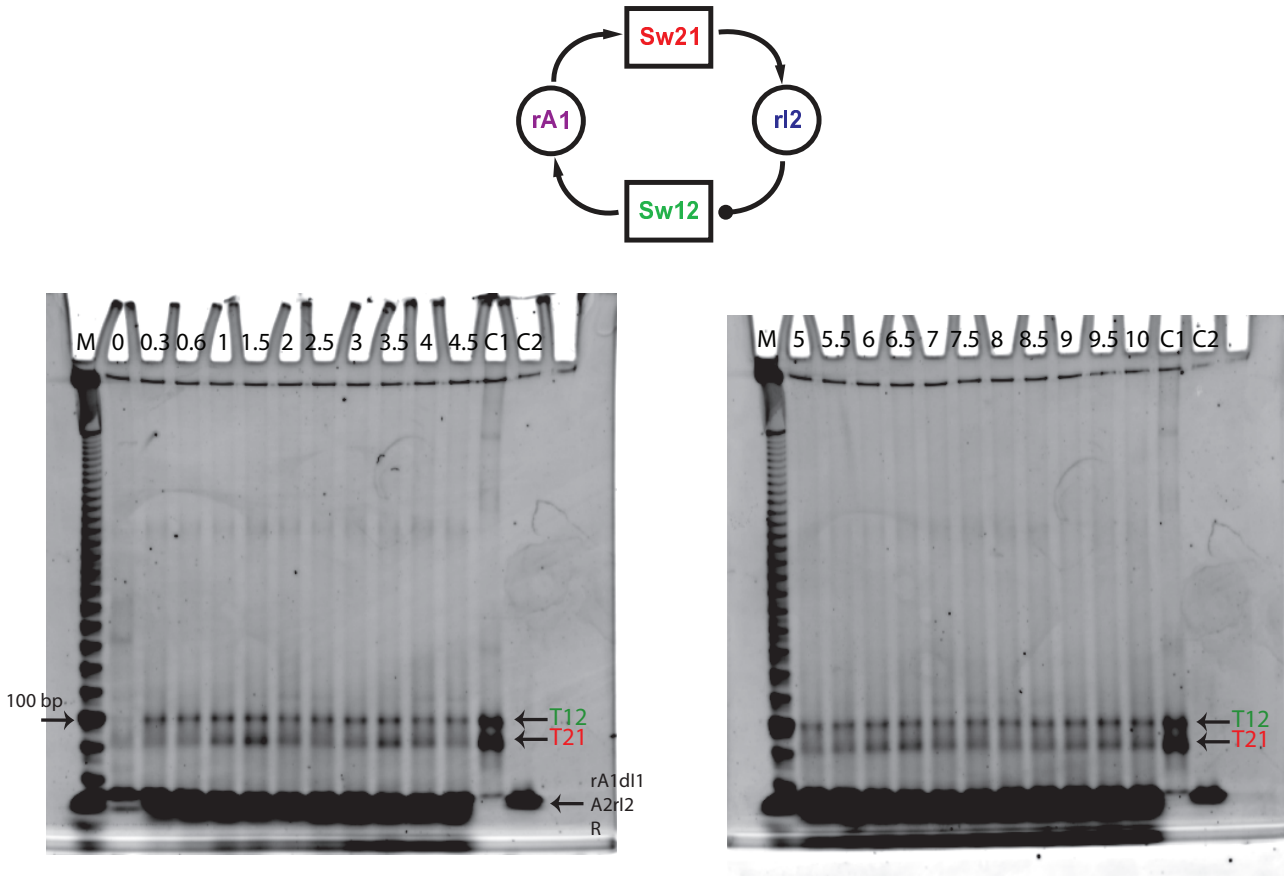

Figure S6: Non-denaturing gel results for the Design I oscillator. The gels are stained with SYBR gold for quantitation. Numbers above each lane mark the transcription reaction times in hours as shown in the fluorescence measurements of Figure 3A. The OFF-state switch concentrations are measured with respect to band densities in control lanes (C1) which contain 1 μM of OFF-state switches, T12 and T21. The ON-state switch templates have low fluorescence due to the quenchers on A1 and A2 (ref. (5)) and are not clearly identified. The rA1dI1 and A2rI2 complexes in control lanes (C2) migrate together at the bottom of the gel. Similarly, other lower molecular weight complexes and single-stranded species are not resolved (R). M: 10 base-pair ladder, C1 and C2: control lanes.

A

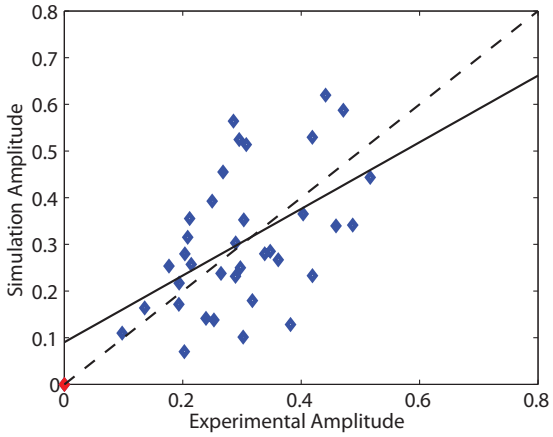
Simulation Amplitude
Experimental Amplitude
0
0.1
0.2
0.3
0.4
0.5
0.6
0.7
0.8
0.2
0.4
0.6

B

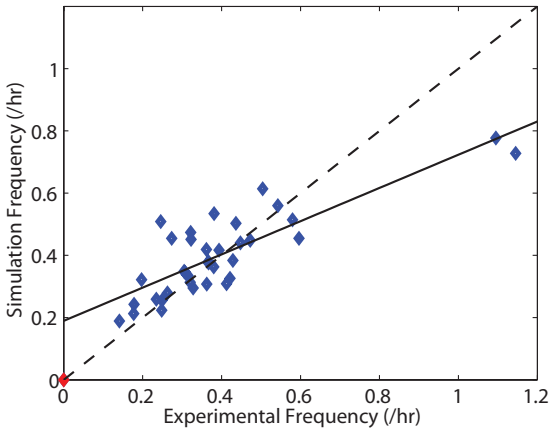
Simulation Frequency (/hr)
Experimental Frequency (/hr)
0
0.2
0.4
0.6
0.8
1
1.2

C

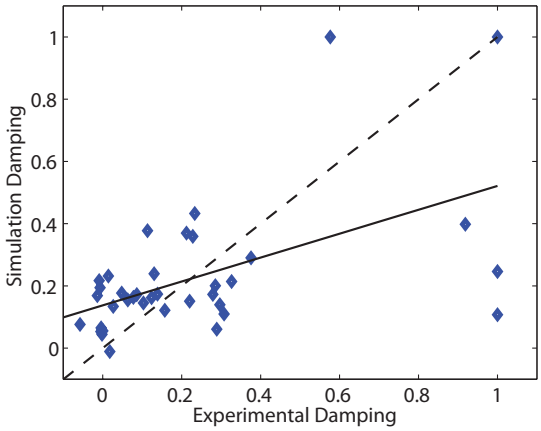
Simulation Damping
Experimental Damping
0
0.2
0.4
0.6
0.8
1

D

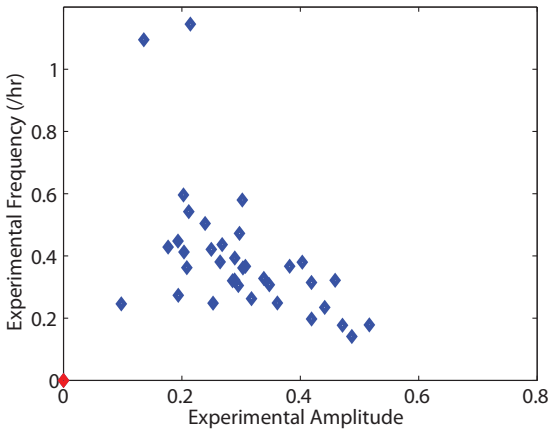
Experimental Frequency (/hr)
Experimental Amplitude
0
0.2
0.4
0.6
0.8
1

E

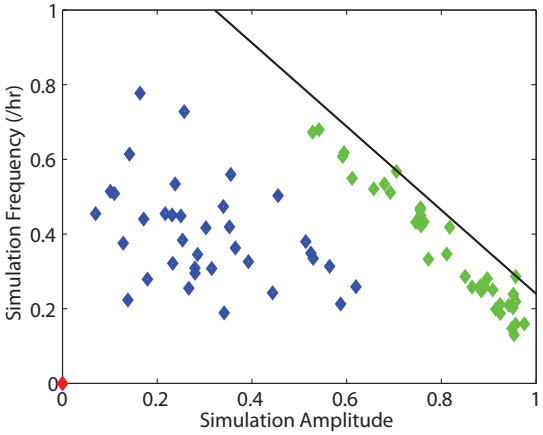
Simulation Frequency (/hr)
Simulation Amplitude
0
0.2
0.4
0.6
0.8
1

Figure S7: Amplitude, frequency, and damping coefficient distribution for experimental results and extended model fits of the Design I oscillator. The amplitude, frequency, and damping coefficient of oscillations are estimated using only the Texas Red fluorescence after the initial transients and prior to the decay of TAMRA signal indicative of energy exhaustion. An example is shown in supplementary text section 3. The amplitude and frequency was not assigned for reaction #22 for both experimental and simulation results, and therefore, reaction #22 was not included in any of the following fit results showing amplitude and frequency (red diamonds at origins in A, B, D, and E). **(A)** Amplitude comparison for experimental and simulation results. The dashed line is an ideal one-to-one correspondence and the black line is a least-squared linear fit result: Simulation Amplitude = 0.71 * Experimental Amplitude + 0.09 ($p = 0.002$). **(B)** Frequency comparison for experimental and simulation results. The dashed line is an ideal one-to-one correspondence and the black line is a least-squared linear fit result: Simulation Frequency = 0.53 * Experimental Frequency + 0.19 ($p < 0.0001$). **(C)** Damping coefficient comparison for experimental and simulation results. The dashed line is an ideal one-to-one correspondence and the black line is a least-squared linear fit result: Simulation Damping Coefficient = 0.38 * Experimental Damping Coefficient + 0.14 ($p = 0.0007$). **(D)** Amplitude and frequency comparison in experimental results. While amplitude and frequency of oscillation can be tuned for various experimental conditions, a sustained oscillation with high amplitude and high frequency is not easy to achieve. **(E)** Amplitude and frequency comparison in simulation results. Similar trend of amplitude and frequency trade-off is observed in the simulation results (blue diamonds). To find a maximum value of amplitude times frequency for each reaction condition, the DNA concentrations ([$T12^{tot}$], [$T21^{tot}$], [$A1^{tot}$], [$dI1^{tot}$], and [$A2^{tot}$]) were allowed to vary between their minimum and maximum values found in reactions #1 through #37, resulting in overall improvements in amplitude and frequency (green diamonds). The enzyme concentrations and rate constants were fixed for each reaction. An apparent amplitude vs frequency trade-off is observed (black line): Simulation Frequency = -1.12 * Simulation Amplitude + 1.36.

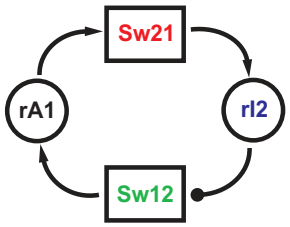

Experiment

Extended model

$k_{s+} = 1.9 \times 10^5$

$k_{s+} = 10^4$

$k_{s+} = 0$

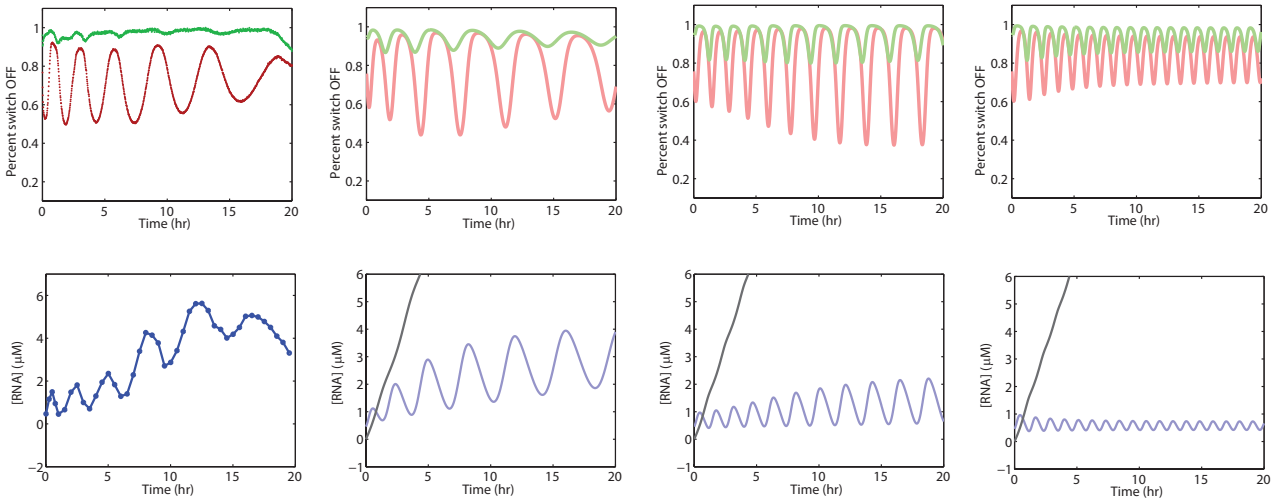

Detailed model

Extended model w/o sI2 generation

$sI2 = 0$

$sI2 = 2\mu M$

$sI2 = 10\mu M$

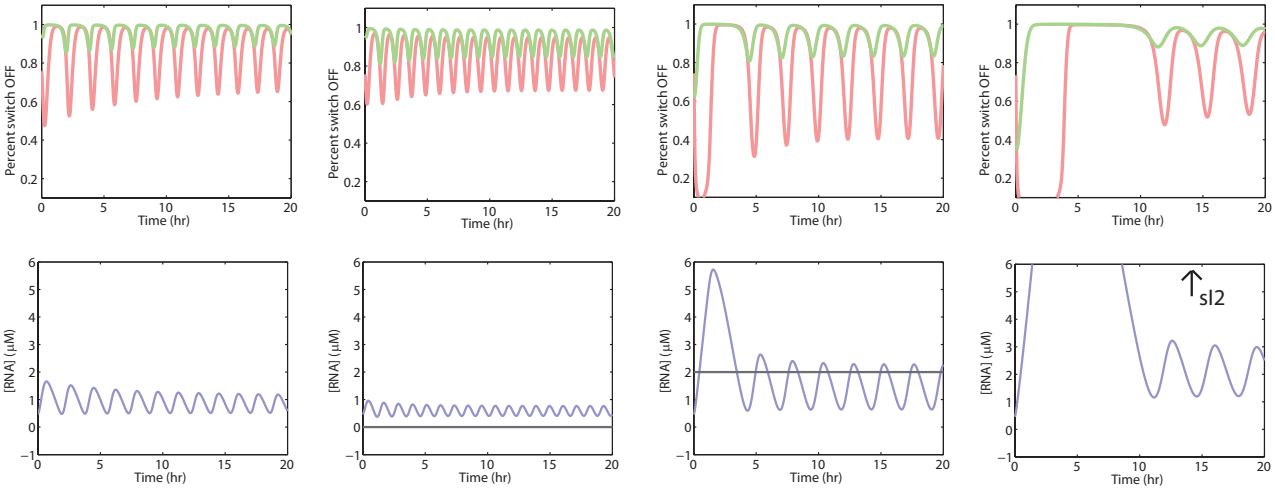

Figure S8: Effect of changing the association rate of incomplete degradation product sI2 in the 'extended model' (see section 1.7). The Texas Red signal of T21 is colored red, the TAMRA signal of T12 is colored green, and the gel-measured concentration of rI2 is colored blue. Same colors are used for simulation results with additional gray lines to indicate the concentration of sI2 as calculated from extended model simulation. Experimental fluorescence time-courses and rI2 concentrations for reaction #37 are plotted, as shown in Figure 3. The experimental conditions are listed in Table S5 and the simulation parameters are listed in Table S2. With a high association rate constant for sI2 ($k_{s,+} = 1.9{*}10^5$/M/s), the mean level of the rI2 oscillation increases over time with concomitant slow-down of the oscillation frequency. At a lower association rate constant ($k_{s,+} = 10^4$/M/s), the oscillations are faster and smaller with less accumulation of rI2. At zero association rate constant ($k_{s,+} = 0$/M/s), the oscillations are even faster and smaller with no accumulation of rI2. An example of the 'detailed model' fit to the experimental result is shown, where the simulated rI2 level shows a good agreement to experimental results only for the initial few hours. We further explored oscillator behavior by assuming that a certain amount of sI2 is provided initially but no further accumulation occurs during the experiment. Simulation results with zero sI2 throughout the reaction showed almost identical behavior to the case with zero association rate of sI2. Higher initial sI2 concentration increased the mean level of the rI2 oscillation and the period of oscillation, but still supported sustained oscillations. (The concentration of sI2 was maintained at 2 μM and 10 μM in these tests.) Sustained rI2 oscillations were observed for sI2 levels as high as 20 μM, which is close to the expected concentration of sI2 after 20 hrs of reaction according to the extended model (data not shown). These simulation results indicate that the interference from incomplete degradation product introduces further delay in the oscillator dynamics and qualitatively changes its behavior, and – more importantly – the oscillator adapts to the sI2 level. Note that the detailed model *does* support sustained oscillations for suitably chosen parameters and concentrations; however, without the extended model reactions, we were unable to simultaneously fit both the fluorescence and gel data from experiments.

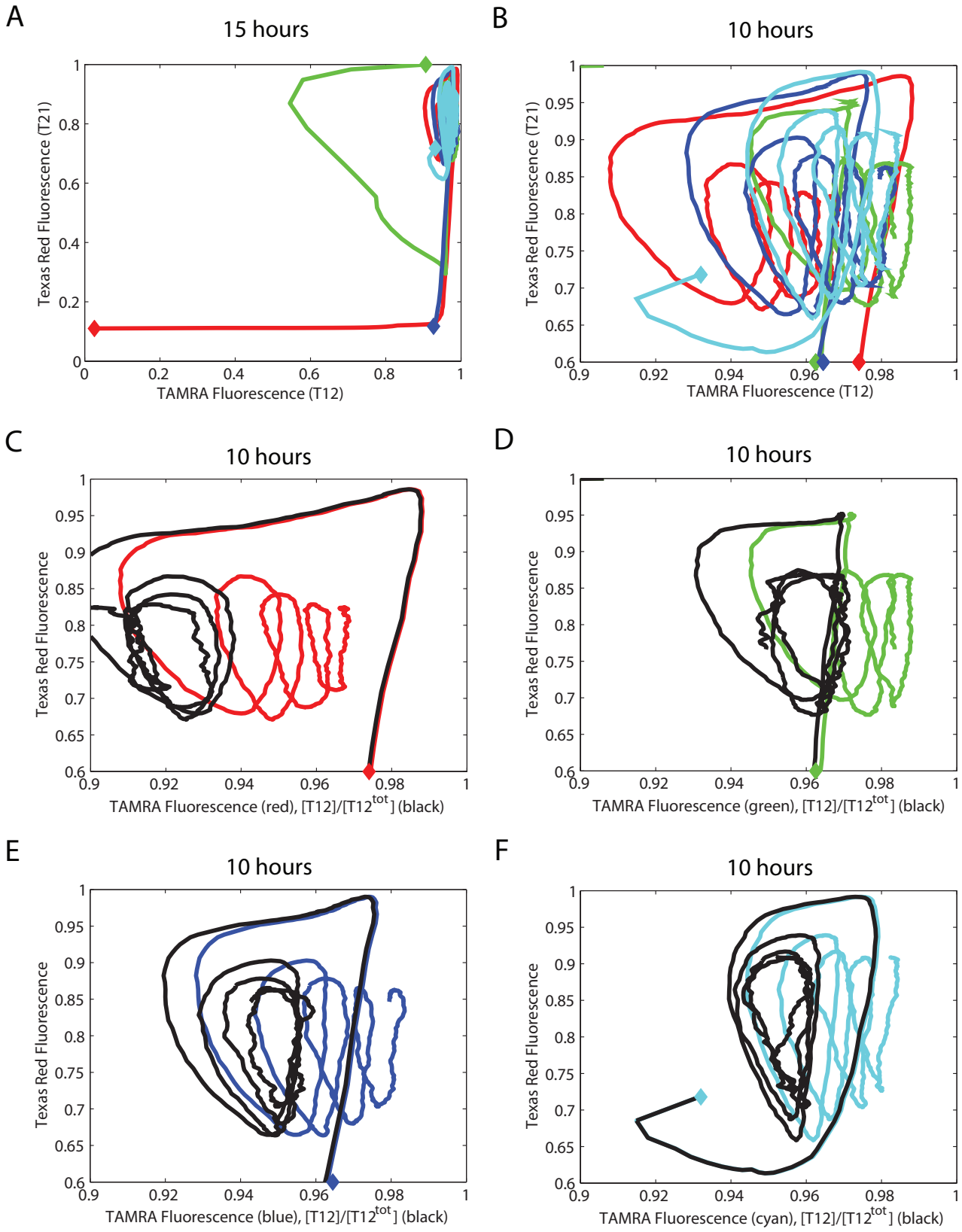
A
15 hours
Texas Red Fluorescence (T21)
TAMRA Fluorescence (T12)
B
10 hours
Texas Red Fluorescence (T21)
TAMRA Fluorescence (T12)
C
10 hours
Texas Red Fluorescence
TAMRA Fluorescence (red), [T12]/[T12tot] (black)
D
10 hours
Texas Red Fluorescence
TAMRA Fluorescence (green), [T12]/[T12tot] (black)
E
10 hours
Texas Red Fluorescence
TAMRA Fluorescence (blue), [T12]/[T12tot] (black)
F
10 hours
Texas Red Fluorescence
TAMRA Fluorescence (cyan), [T12]/[T12tot] (black)

Figure S9: Phase plane trajectories of the Design I oscillator with four different initial RNA input combinations. The DNA and enzyme concentrations were identical for these reactions. For visualization purposes, the experimental trajectories were smoothed by taking a moving average of 20 data points taken every minute. **(A)** Four sets of RNA input combinations were used to place the initial conditions at four different points in the phase plane. Experimental data from reactions #33 through #36 of the Design I oscillator (Table S5 and Figure S4) are shown (reaction #33: red, reaction #34: green, reaction #35: blue, and reaction #36: cyan). The data points for the first 15 hours of experimental observations are shown with the initial points marked by diamonds. **(B)** An expanded view of the phase plane. For clarity, the data points for only the initial 10 hours of experimental observations are shown. The trajectories from different initial conditions approach a similar damped-but-drifting limit cycle oscillation. The first entry points of trajectories within the expanded phase plane are marked by diamonds. **(C-F)** The simulation results of the extended model makes it unlikely that the drift in the TAMRA fluorescence is due to a change of dynamics by accumulation of short degradation products, sI2. Instead, to explain the signal drift, we re-examine our assumption (used throughout the rest of the paper) that fluorescence signals (normalized to 0 and 1 as described in Methods) directly correspond to the percentage of activated switches. We hypothesized that the accumulating sI2, by reversibly binding to the ON-state switch T12A2, can reduce the effective quenching (by quenchers on the activator strands) and increase the signal of the ON-state switch. We therefore investigated whether a quantitative model of this effect could explain the drift. To wit, $TAM = \frac{[\mathrm{T12}]}{[\mathrm{T12^{tot}}]} + \frac{[\mathrm{T12A2}]}{[\mathrm{T12^{tot}}]} * \alpha * [\mathrm{sI2}] = \frac{[\mathrm{T12}]}{[\mathrm{T12^{tot}}]} * (1 - \alpha * [\mathrm{sI2}]) + \alpha * [\mathrm{sI2}]$, $\frac{[\mathrm{T12}]}{[\mathrm{T12^{tot}}]} = \frac{TAM - \alpha * [\mathrm{sI2}]}{1 - \alpha * [\mathrm{sI2}]}$, where TAM is normalized TAMRA fluorescence and α is a fit parameter to reflect change of T12A2 fluorescence signal. Here, the concentration of sI2 at any given time is calculated from the extended model simulation. Given α, the TAM signal can be used to back-calculate an inferred 'corrected' T12 concentration. We found that choosing $\alpha = 1/24.5$ μM for all four trajectories allowed relatively constant inferred 'corrected' T12 level after each oscillation cycle. The trajectories for 10 hours of reaction #33 (C), #34 (D), #35 (E), and #36 (F) within the expanded phase plane are shown. The experimental data are shown in colors, while the calculated T12 concentrations are shown in black. Although this back-calculation is not used elsewhere in this work to correct the T12 measurements, it is reasonable to think that they could be more accurate.

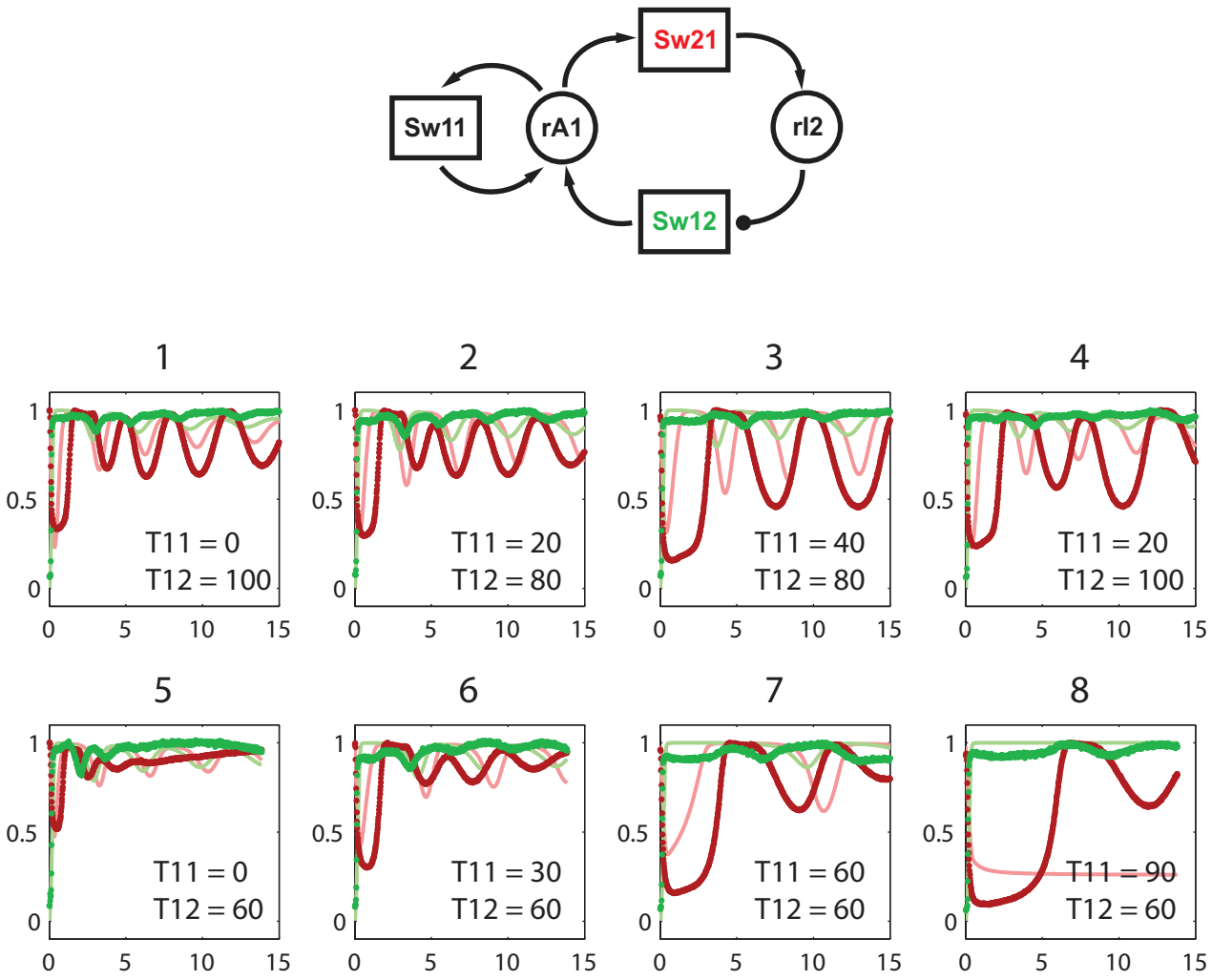

Figure S10: Experimental results and extended model fits for the amplified negative feedback oscillator (Design II). Horizontal axes are time in hours, and vertical axes are normalized fluorescence signal. The experimental time-courses are plotted as dots and simulation time-courses are plotted as lines in lighter shades: Texas Red of T21 (red) and TAMRA of T12 (green). To generate simulation time-courses, we used the parameter set listed in Table S3. These parameters were fit using the fluorescence time-courses of the Design II oscillator. We omitted reaction #8 during the fit because the simulation result predicted bistable behavior for reaction #8 for a wide range of parameter choices. The experimental conditions are listed in Table S6 with the corresponding reaction numbers indicated above each plot. We explored different combinations of T11 and T12 concentrations as marked in each plot. For reactions #5 through #8, the concentration of T11 was sequentially increased by 30 nM from 0 nM up to 90 nM, while all the other DNA and enzyme concentrations were held constant. Reactions #5, #6 and #8 are shown in Figure 4.

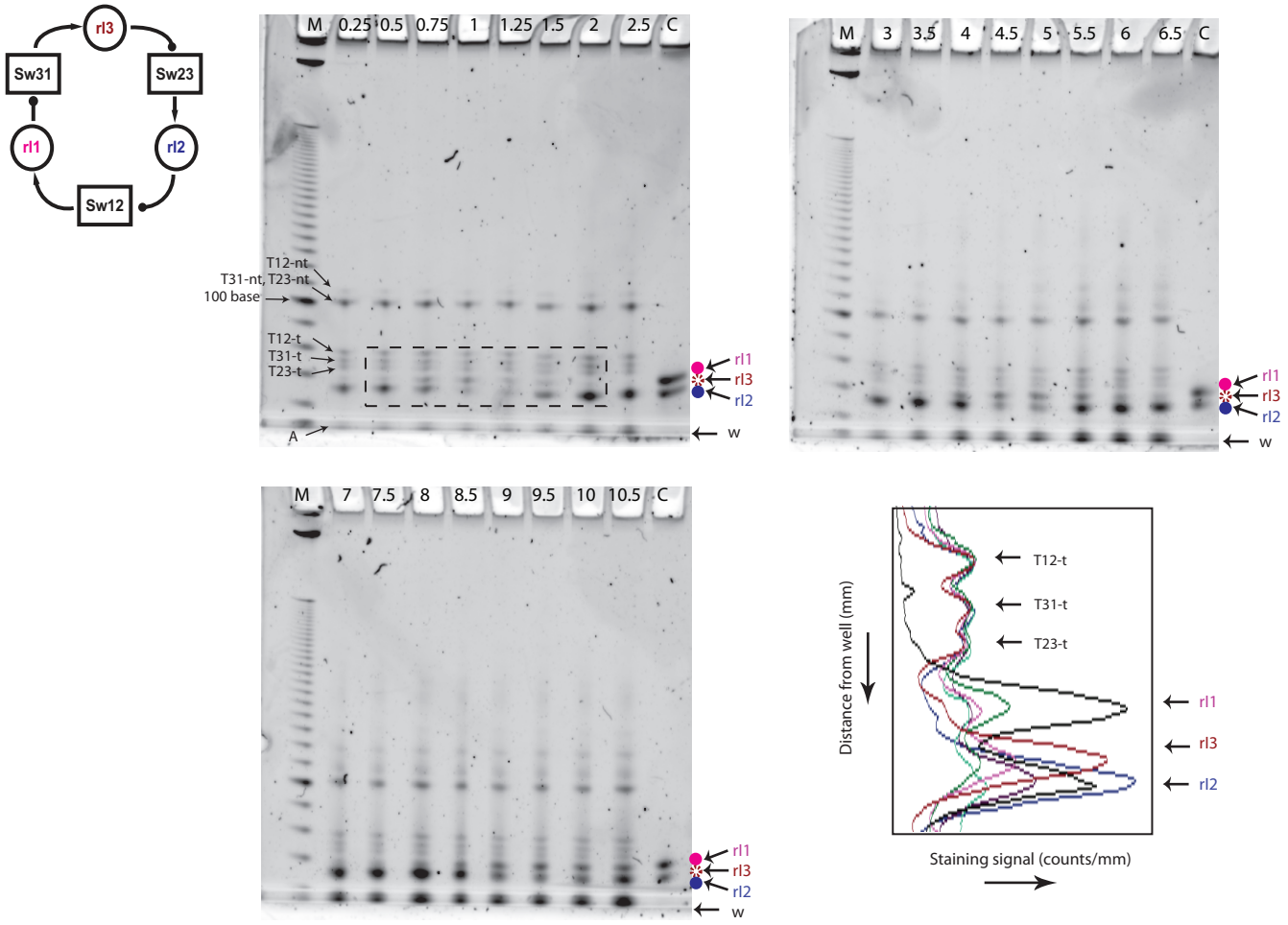

Figure S11: Gel results for the three-switch ring oscillator (Design III). The denaturing gel is stained with SYBR gold for quantitation. Numbers above each lane mark the transcription reaction times in hours as shown in the fluorescence measurements of Figure 5A. The RNA inhibitor concentrations were measured with respect to reference band densities in control lanes which contain 1 μM of purified rI1 (67 bases, identical sequence to rA1 in Design I oscillator) and rI2 (62 bases). The inhibitor rI3 (64 bases) was not included in the control lanes (dotted circle). For normalization, the rI3 reference signal was assumed to be the mean of the rI1 and rI2 reference signals. To find the location of the rI3 band between those of the rI1 and rI2 bands, enlarged lane profiles were analyzed as shown in the bottom right panel, which plots the staining intensity for the six lanes in the dotted area in the top left gel. Alignment of lane profiles based on three template strands (T12-t, T31-t, and T23-t) could assign the RNA peaks to rI1, rI2, and rI3, and these RNA bands were well-modeled by 5-pixel wide Gaussian peaks. When compared with the control lane (black), lanes at hour 0.5 through hour 1 have rI3 bands (red, magenta, green), while lanes at hour 1.25 through hour 2 have rI2 bands (cyan, purple, blue). Using the alignment results to assign the center locations of rI1 and rI3 to be 15 pixels apart and those of rI1 and rI2 to be 20 pixels apart, the heights of all three Gaussian peaks were simultaneously fit using Matlab. The DNA strands were also identified: T12-nt (106 bases), T31-nt (103 bases), T23-nt (101 bases), T12-t (79 bases), T31-t (76 bases), and T23-t (74 bases). The strand T23-t is identical to T21-t of the Design I oscillator, and the band of T31-nt and the band of T23-nt overlap. The DNA activators (A) were not clearly identified because they almost run off of the gel. The unresolved bands at the bottom of the gel also include presumed incomplete degradation products (w). M: 10 base-pair ladder, C: control lane.

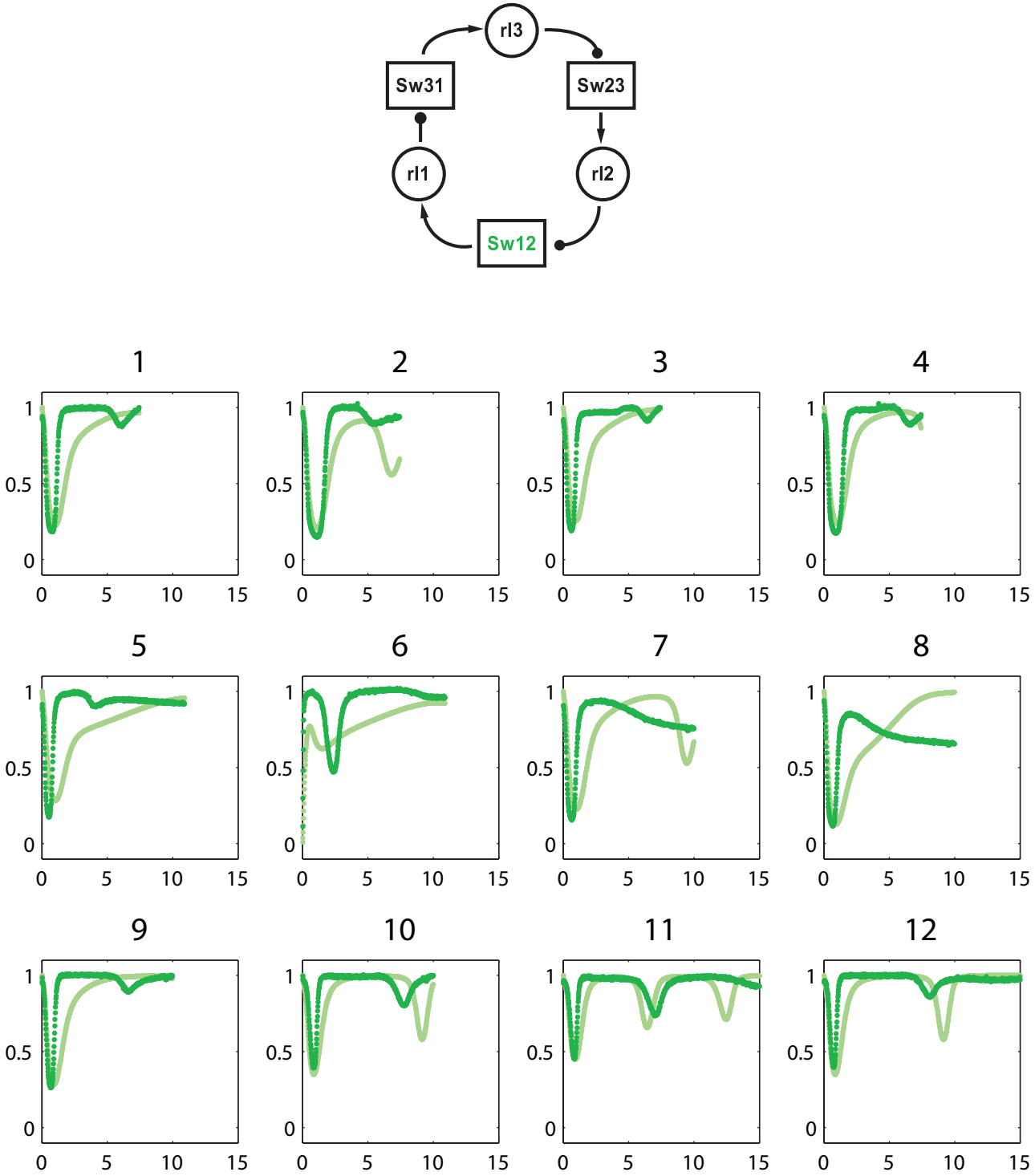

Figure S12: Experimental results and extended model fits for the three-switch ring oscillator (Design III). Horizontal axes are time in hours, and vertical axes are normalized fluorescence signal. The experimental time-courses for the TAMRA signal from switch Sw12 are plotted as green dots and simulation time-courses are plotted as light green lines. The two other switches were not measured by fluorescence. To generate simulation time-courses, we used the parameter set listed in Table S4. These parameters were fit using the fluorescence time-courses and gel data for the Design III oscillator. The experimental conditions are listed in Table S7 with the corresponding reaction numbers indicated above each plot. Reaction #27 is shown in Figure 5.

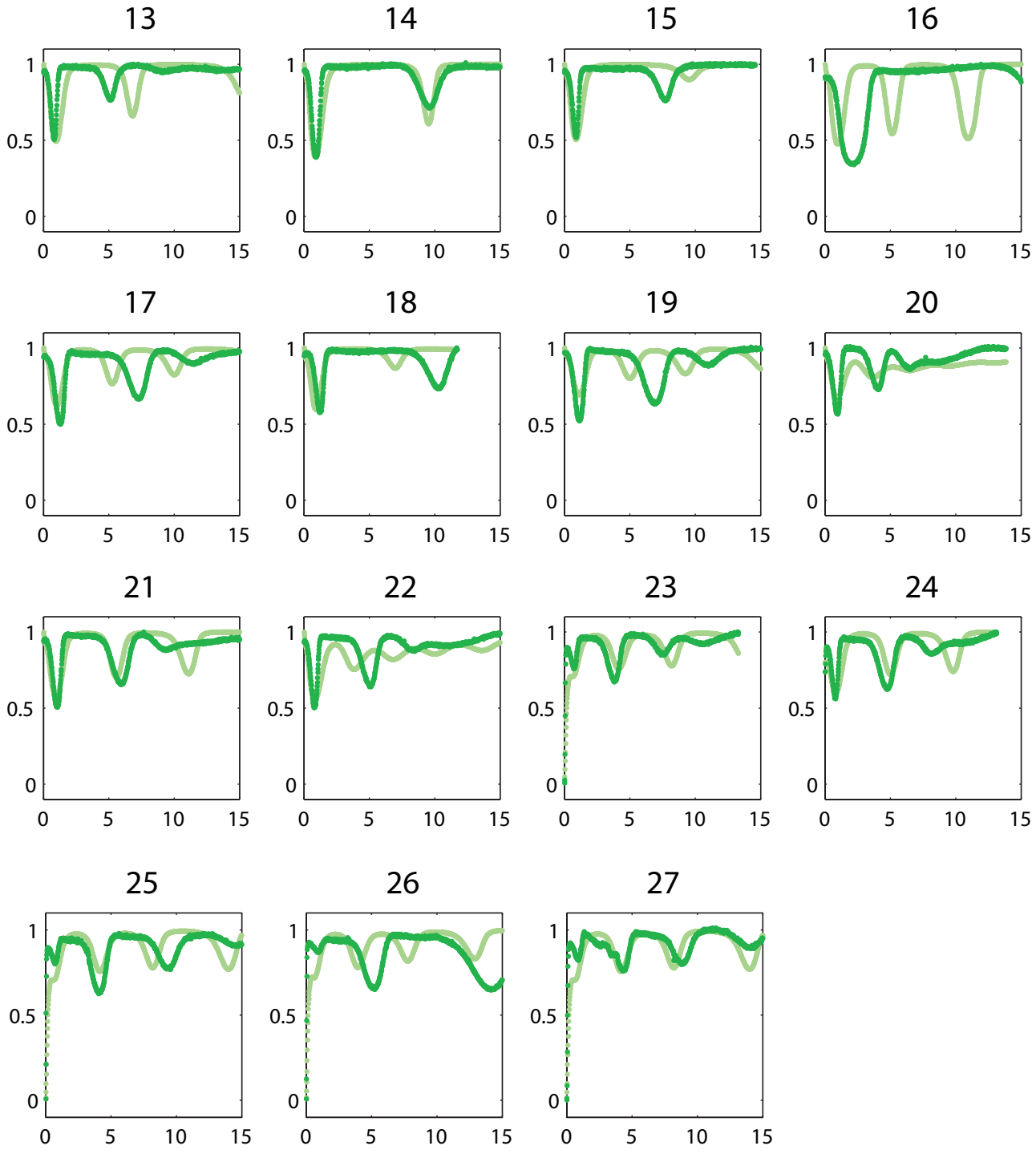
13
14
15
16
17
18
19
20
21
22
23
24
25
26
27
0
0.5
1
0
5
10
15